Engineering & Technology in India

www.engineeringandtechnologyinindia.com

Strength for Today and Bright Hope for Tomorrow

Volume 1:2 March 2016

Chief Editor
D. Nagarathinam, M.E., Ph.D.

Editors
Dr. P. N. Rajnarayanan, M.E., Ph.D.
Dr. K. Sudalaimani, M.E., Ph.D.
Dr. S. Ramanathan, Ph.D.

Language and Style Advisors
G. Baskaran, Ph.D.
Sam Mohanlal, Ph.D.

Executive Editor
M. S. Thirumalai, Ph.D.

Contents

==========
Engineering & Technology in India www.engineeringandtechnologyinindia.com
Vol. 1:2 March 2016
==========

BENDS ONLY, NOT THE END

Jimmy Teo
Philosopher, Motivator and Entrepreneur

Life is always in the forward gear until the end
All problems are necessary bends;
Without bitterness, sweetness has less contents
Without stormy weather, the bright sunshine is just a blank.

Add 'b' to 'end', and we have 'bend'
That 'curve or sharp' bend necessary to slow us
To be safe & have adequate rest
Or burn out & suffer before the 'end'.

Add 'f' to 'end' and we have 'fend'
That mandatory personal self-effort
To move against laziness & dependence on others & parents
And be self-supporting; inspiring others likewise.

Add 'l' to 'end' and we have 'lend'
It is good if we could lend or help the poor,
Instead of borrowing from others;
As helping the poor is lending to the Lord.

Add 'm' to 'end' and we have 'mend'
That sincere & loving efforts to mend our ways
To be better & humbler
And to be exemplary for others.

Add 'r' to end and we have 'rend'
To pull asunder or tear apart everything wrong
Both within or without;
Daring to speak & fight for the rights of the poor & underprivileged.

Add 's' to end and we have 'send'
The art of relaying & sending good inspirations
To all our friends, even financial support for genuine needy
Especially for kids, so that they could have a good future.

Add 't' to 'end' and we have 'tend'
That tender touch to tend to whatever we have
With simplicity & purity
So that we have less complication & difficulties.

Add 'v' to 'end' and we have 'vend'
That ability to provide, like a vending machine
For ourselves & loved ones
Through prudent sufficient savings rather than to be dependent on others.

A Note by the Author:

8.22am/Mon/8.6.15/On board SQ 998 to Yangon

NB: Mark Chua, my associate from EASB suggested (he was seated next to me on the plane, the very 1st person to see my draft as I penned on the plane) that when I add 'Fri' to the 'end', we have 'friend'. Indeed so. Let ‘Friday’ be the day for us to take time to enjoy quality time with friends (our progenies are our friends as well, as in some families they are not so). It is the start of the weekend. We need rest. We need replenishment of warmth & inspiration.

Jimmy Teo
Philosopher, Motivator and Entrepreneur
Singapore
teojimmy07@gmail.com

==========
Engineering & Technology in India www.engineeringandtechnologyinindia.com
Vol. 1:2 March 2016
==========

FEATURES EXTRACTION IN CONTEXT BASED IMAGE RETRIEVAL

A project report submitted by

ARAVINDH A S

J CHRISTY SAMUEL

in partial fulfilment for the award of the degree of

BACHELOR OF TECHNOLOGY

in

ELECTRONICS AND COMMUNICATION ENGINEERING

under the supervision of

Mrs. M. A. P. MANIMEKALAI, M.E.

SCHOOL OF ELECTRICAL SCIENCES
KARUNYA UNIVERSITY
(Karunya Institute of Technology and Sciences)
(Declared as Deemed to be University under Sec-3 of the UGC Act, 1956)
Karunya Nagar, Coimbatore - 641 114, Tamilnadu, India

APRIL 2015

BONA FIDE CERTIFICATE

Certified that this project report "Features Extraction in Context Based Image Retrieval" is the bona fide work of ARAVINDH A S (UR11EC014), and CHRISTY SAMUEL J. (UR11EC026) who carried out the project work under my supervision during the academic year 2014-2015.

Mrs. M. A. P. MANIMEKALAI, M.E
SUPERVISOR
Assistant Professor
Department of ECE
School of Electrical Sciences

Dr. SHOBHA REKH, M.E., Ph.D.,
HEAD OF THE DEPARTMENT
Professor
Department of ECE
School of Electrical Sciences

ACKNOWLEDGEMENT

First and foremost, we praise and thank **ALMIGHTY GOD** whose blessings have bestowed in us the will power and confidence to carry out our project. We are grateful to our most respected Founder (late) **Dr. D.G.S. DHINAKARAN**, **C.A.I.I.B, Ph.D.,** and Honourable Chancellor **Dr. PAUL DHINAKARAN**, **M.B.A., Ph.D.** for their grace and blessing.

We extend our thanks to our Honourable Vice-chancellor **Dr. S. SUNDAR MANOHARAN, Ph.D.** and our respected Registrar **Dr. C. JOSEPH KENNEDY, Ph.D.,** for the opportunity given to us to take up the project.

We extend our thanks to **Dr. SHOBHA REKH, M.E., Ph.D., Professor and Head of the Department of ECE** for her encouragement and guidance. We are indebted to our supervisor **Mrs. M.A.P.MANIMEKALAI, M.E. Assistant Professor**, for her valuable support, advice and encouragement.

We would like to thank the project coordinators for their support in all the project reviews. We also thank all the staff members of our department for extending their helping hands to make this project a success.

We would also like to thank all our friends and beloved parents who prayed and helped us during the project work.

Aravindh A.S.

J. Christy Samuel

ABSTRACT

There has been a growing interest in exploiting contextual information in addition to local features to detect and localize multiple object categories in an image. A context model can rule out some unlikely combinations or locations of objects and guide detectors to produce a semantically coherent interpretation of a scene. Our model incorporates global image features, dependencies between object categories, and outputs of local detectors into one probabilistic framework. We demonstrate that our context model improves object recognition performance and provides a coherent interpretation of a scene, which enables a reliable image querying system by multiple object categories. In addition, our model can be applied to scene understanding tasks that local detectors alone cannot solve, such as detecting objects out of context or querying for the most typical and the least typical scenes in a data set.

Key words: image retrieval, context-based extraction, querying system, localization.

TABLE OF CONTENTS

LIST OF TABLES

LIST OF FIGURES

LIST OF ABBREVATIONS/ ACRONYMS

SURF - SPEEDED UP ROBUST FEATURE

SIFT - SCALE INVARIENT FEATURE TRANSFORM

CHAPTER-1

INTRODUCTION

1.1 Edge Detection:

Edge detection is the name for a set of mathematical methods which aim at identifying points in a digital image at which the image brightness changes sharply or, more formally, has discontinuities. The points at which image brightness changes sharply are typically organized into a set of curved line segments termed edges. The same problem of finding discontinuities in 1D signals is known as step detection and the problem of finding signal discontinuities over time is known as change detection. Edge detection is a fundamental tool in image processing, machine vision and computer vision, particularly in the areas of feature detection and feature extraction.

The purpose of detecting sharp changes in image brightness is to capture important events and changes in properties of the world. It can be shown that under rather general assumptions for an image formation model, discontinuities in image brightness are likely to correspond to:

i) Discontinuities in depth
ii) Discontinuities in surface orientation,
iii) Changes in material properties and
iv) Variations in scene illumination.

1.2 Objective:

In the ideal case, the result of applying an edge detector to an image may lead to a set of connected curves that indicate the boundaries of objects, the boundaries of

surface markings as well as curves that correspond to discontinuities in surface orientation. Thus, applying an edge detection algorithm to an image may significantly reduce the amount of data to be processed and may therefore filter out information that may be regarded as less relevant, while preserving the important structural properties of an image. If the edge detection step is successful, the subsequent task of interpreting the information contents in the original image may therefore be substantially simplified. However, it is not always possible to obtain such ideal edges from real life images of moderate complexity.

Edges extracted from non-trivial images are often hampered by fragmentation, meaning that the edge curves are not connected, missing edge segments as well as false edges not corresponding to interesting phenomena in the image – thus complicating the subsequent task of interpreting the image data.

Edge detection is one of the fundamental steps in image processing, image analysis, image pattern recognition, and computer vision techniques.

1.3 Aim and Objective of the Research:

The aim of the project is:

i) To know the working of the SIFT and SURF
ii) Image Properties using SIFT and SURF
iii) To the difference of these both image features

CHAPTER 2

LITERATURE SURVEY

We develop an efficient framework to exploit contextual information in object recognition and scene understanding problems by modeling object dependencies, global image features, and local detector outputs using a tree-based graphical model. Our context model enables a parsimonious modeling of object dependencies, and can easily scale to capture the dependencies of over 100 object categories. The SUN 09 data set presented in this paper has richer contextual information than PASCAL 07, and is more suitable for training and evaluating context models. We demonstrate that our context model learned from SUN 09 significantly improves the accuracy of object recognition and image query results, and can be applied to find objects out of context (The SUN 09 data set and the Matlab implementation of our algorithm). We conclude by discussing some possible extensions of the work presented in this paper. Our location model captures spatial relationships of object categories using Gaussian distributions. While this greatly reduces computational complexity, it does not capture some physical relationships such as a car is supported by a road. In addition, the location model can be improved by encoding different types of interactions or poses among object instances (e.g., person 1 is riding a horse and person 2 is standing next to it), or spatial relationships based on different viewpoints . The tree structure shown in Fig. 6 captures the inherent hierarchy among object categories. For example, most of the objects that commonly appear in a kitchen are descendants of the node sink, and all the vehicles are descendants of road. This suggests that a more intuitive structure for object dependencies could be a hierarchy including some metaobjects (such as a desk area) or scenes (kitchen or street) as nodes at coarser scales. Learning a full hierarchical tree structure with such additional nodes may

discover important relationships among objects, metaobjects, and scenes, which is an interesting direction for further research.

A simple form of contextual information is a co-occurrence frequency of a pair of objects. Rabinovich et al. use local detectors to first assign an object label to each image segment, and then adjusts these labels using a conditional random field (CRF). This approach is extended in and to encode spatial relationships between a pair of objects. In spatial relationships are quantized to four prototypical relationships—above, below, inside, and around, whereas in a nonparametric map of spatial priors is learned for each pair of objects. Torralba et al.combine boosting and CRFs to first detect easy objects (e.g., a monitor) and pass the contextual information to detect other more difficult objects (e.g., a keyboard). Tu uses both image patches and their probability maps estimated from classifiers to learn a contextual model, and iteratively refines the classification results by propagating the contextual information. Desai et al.combine individual classifiers by using spatial interactions between object detections in a discriminative manner. Contextual information may be obtained from coarser, global features as well. Torralba demonstrates that a global image feature called “gist” can predict the presence or absence of objects and their locations without running an object detector. This is extended in to combine patch-based local features and the gist feature. Heitz and Koller combine a sliding window method and unsupervised image region clustering to leverage “stuff”such as the sea, the sky, or a road to improve object detection. A cascaded classification model in links scene categorization, multiclass image segmentation, object detection, and 3D reconstruction.

CHAPTER 3

DESIGN METHEODOLOGY

3.1 Description

Image registration is critical task in many applications. To perform image registration/alignment, required steps are: Feature detection, Feature matching, derivation of transformation function based on corresponding features in images and reconstruction of images based on derived transformation function. Accuracy of registered image depends on accurate feature detection and matching. So these two intermediate steps are very important in many image applications: image registration, computer vision, image mosaic etc. This paper presents two different methods for scale and rotation invariant interest point/feature detector and descriptor: Scale Invariant Feature Transform (SIFT) and Speed Up Robust Features (SURF). It also presents a way to extract distinctive invariant features from images that can be used to perform reliable matching between different views of an object/scene

3.2 Process Stages

3.2.1 Types of Edge Detection and Feature Extraction

1. Sobel Edge Detector
2. Canny Edge Detector
3. Prewitt Edge Detector
4. SURF
5. SIFT

3.2.2 Sobel Edge Detector

The Sobel operator, sometimes called Sobel Filter, is used in image processing and computer vision, particularly within edge detection algorithms, and creates an image which emphasizes edges and transitions. It is named after Irwin Sobel, who presented the idea of an "Isotropic 3x3 Image Gradient Operator" at a talk at the Stanford Artificial Intelligence Project (SAIP) in 1968. Technically, it is a discrete differentiation operator, computing an approximation of the gradient of the image intensity function. At each point in the image, the result of the Sobel operator is either the corresponding gradient vector or the norm of this vector. The Sobel operator is based on convolving the image with a small, separable, and integer valued filter in horizontal and vertical direction and is therefore relatively inexpensive in terms of computations. On the other hand, the gradient approximation that it produces is relatively crude, in particular for high frequency variations in the image. The Kayyali operator for edge detection is another operator generated from Sobel operator.

The operator uses two 3×3 kernels which are convolved with the original image to calculate approximations of the derivatives - one for horizontal changes, and one for vertical. If we define A as the source image, and Gx and Gy are two images which at each point contain the horizontal and vertical derivative approximations, the computations are as follows:

$$G_y = \begin{bmatrix} -1 & -2 & -1 \\ 0 & 0 & 0 \\ +1 & +1 & +1 \end{bmatrix} * A \ \ and \ \ G_x = \begin{bmatrix} -1 & 0 & +1 \\ -2 & 0 & +2 \\ -1 & 0 & +1 \end{bmatrix} \qquad ----\rightarrow 1$$

where * here denotes the 2-dimensional convolution operation.

Since the Sobel kernels can be decomposed as the products of an averaging and a differentiation kernel, they compute the gradient with smoothing. For example, can be written as

$$\begin{bmatrix} -1 & 0 & +1 \\ -2 & 0 & +2 \\ -1 & 0 & +1 \end{bmatrix} = \begin{bmatrix} 1 \\ 2 \\ 1 \end{bmatrix} [-1 \quad 0 \quad +1] \qquad ---\rightarrow 2$$

The x-coordinate is defined here as increasing in the "right"-direction, and the y-coordinate is defined as increasing in the "down"-direction. At each point in the image, the resulting gradient approximations can be combined to give the gradient magnitude, using:

$$G = \sqrt{G_x^2 + G_y^2} \qquad ---\rightarrow 3$$

Using this information, we can also calculate the gradient's direction:

$$\theta = atan2(G_y, G_x) \qquad ---\rightarrow 4$$

where, for example, θ is 0 for a vertical edge which is lighter on the right side.

As a consequence of its definition, the Sobel operator can be implemented by simple means in both hardware and software: only eight image points around a point are needed to compute the corresponding result and only integer arithmetic is needed to compute the gradient vector approximation. Furthermore, the two discrete filters described above are both separable:

$$\begin{bmatrix} 1 & 0 & -1 \\ 2 & 0 & -2 \\ 1 & 0 & -1 \end{bmatrix} = \begin{bmatrix} 1 \\ 2 \\ 1 \end{bmatrix} [-1 \quad 0 \quad -1] = \begin{bmatrix} 1 \\ 1 \end{bmatrix} * \begin{bmatrix} 1 \\ 1 \end{bmatrix} [1 \quad -1] * [1 \quad 1] \qquad ---\rightarrow 5$$

$$\begin{bmatrix} 1 & 2 & 1 \\ 0 & 0 & 0 \\ 1 & 0 & -1 \end{bmatrix} = \begin{bmatrix} 1 \\ 0 \\ -1 \end{bmatrix} [1 \quad 2 \quad 1] = \begin{bmatrix} 1 \\ -1 \end{bmatrix} * \begin{bmatrix} 1 \\ -1 \end{bmatrix} [1 \quad 1] * [1 \quad 1] \qquad ---\rightarrow 6$$

$$G_x = \begin{bmatrix} 1 \\ 2 \\ 1 \end{bmatrix} * ([-1 \quad 0 \quad -1] * A) \quad and \quad G_y = \begin{bmatrix} 1 \\ 0 \\ -1 \end{bmatrix} * ([1 \quad 2 \quad 1] * A) \quad ----\rightarrow 7$$

Since the intensity function of a digital image is only known at discrete points, derivatives of this function cannot be defined unless we assume that there is an underlying continuous intensity function which has been sampled at the image points. With some additional assumptions, the derivative of the continuous intensity function can be computed as a function on the sampled intensity function, i.e. the digital image. It turns out that the derivatives at any particular point are functions of the intensity values at virtually all image points. However, approximations of these derivative functions can be defined at lesser or larger degrees of accuracy.

The Sobel operator represents a rather inaccurate approximation of the image gradient, but is still of sufficient quality to be of practical use in many applications. More precisely, it uses intensity values only in a 3×3 region around each image point to approximate the corresponding image gradient, and it uses only integer values for the coefficients which weight the image intensities to produce the gradient approximation.

3.2.3 Canny Edge Detector

The Canny edge detector is an edge detection operator that uses a multi-stage algorithm to detect a wide range of edges in images. It was developed by John F. Canny in 1986. Canny also produced a computational theory of edge detection explaining why the technique works

Edge detection, especially step edge detection has been widely applied in various different computer vision systems, which is an important technique to extract useful structural information from different vision objects and dramatically reduce the amount

of data to be processed. Canny has found that, the requirements for the application of edge detection on diverse vision systems are relatively the same. Thus, a development of an edge detection solution to address these requirements can be implemented in a wide range of situations. The general criteria for edge detection includes

1. Detection of edge with low error rate, which means that the detection should accurately catch as many edges shown in the image as possible
2. The edge point detected from the operator should accurately localize on the center of the edge.
3. A given edge in the image should only be marked once, and where possible, image noise should not create false edges.

To satisfy these requirements Canny used the calculus of variations – a technique which finds the function which optimizes a given functional. The optimal function in Canny's detector is described by the sum of four exponential terms, but it can be approximated by the first derivative of a Gaussian.

Among the edge detection methods developed so far, canny edge detection algorithm is one of the most strictly defined methods that provides good and reliable detection. Owing to its optimality to meet with the three criteria for edge detection and the simplicity of process for implementation, it becomes one of the most popular algorithms for edge detection.

Process Edge Detection Algorithm of Canny:

The Process of Canny edge detection algorithm can be broken down to 5 different steps:

1. Apply Gaussian filter to smooth the image in order to remove the noise

2. Find the intensity gradients of the image
3. Apply non-maximum suppression to get rid of spurious response to edge detection
4. Apply double threshold to determine potential edges
5. Track edge by hysteresis: Finalize the detection of edges by suppressing all the other edges that are weak and not connected to strong edges.

Every step will be described in details as following. The introduction of procedure below is developed based on Prof Thomas Moeslund's lecture note for digital image processing in Indian Institute of Technology.

Non-maximum suppression is an edge thinning technique.

Non-Maximum suppression is applied to "thin" the edge. After applying gradient calculation, the edge extracted from the gradient value is still quite blurred. With respect to criteria 3, there should only be one accurate response to the edge. Thus non-maximum suppression can help to suppress all the gradient values to 0 except the local maximal, which indicates location with the sharpest change of intensity value. The algorithm for each pixel in the gradient image is:

1. Compare the edge strength of the current pixel with the edge strength of the pixel in the positive and negative gradient directions.

2. If the edge strength of the current pixel is the largest compared to the other pixels in the mask with the same direction(i.e, the pixel that is pointing in the y direction, it will be compared to the pixel above and below it in the vertical axis), the value will be preserved. Otherwise, the value will be suppressed.

Double Threshold

After application of non-maximum suppression, the edge pixels are quite accurate to present the real edge. However, there are still some edge pixels at this point caused by noise and color variation. In order to get rid of the spurious responses from these bothering factors, it is essential to filter out the edge pixel with the weak gradient value and preserve the edge with the high gradient value. Thus two threshold values are set to clarify the different types of edge pixels, one is called high threshold value and the other is called the low threshold value. If the edge pixel's gradient value is higher than the high threshold value, they are marked as strong edge pixels. If the edge pixel's gradient value is smaller than the high threshold value and larger than the low threshold value, they are marked as weak edge pixels. If the pixel value is smaller than the low threshold value, they will be suppressed. The two threshold values are empirically determined values, which will need to be defined when applying to different images.

Edge Tracking by Hysteresis

So far, the strong edge pixels should certainly be involved in the final edge image, as they are extracted from the true edges in the image. However, there will be some debate on the weak image pixels, as these pixels can either be extracted from the true edge, or the noise/color variations. To achieve an accurate result, the weak edges caused from the latter reasons should be removed. The criteria to determine which case does the weak edge belongs to, is that usually the weak edge pixel caused from true edges will be connected to the strong edge pixel. To track the edge connection, Binary Large Object-analysis is applied by looking at a weak edge pixel and its 8-connected neighborhood pixels. As long as there is one strong edge pixel is involved in the BLOB, that weak edge point can be identified as one that should be preserved

Improvement on Canny Edge Detection:

While traditional canny edge detection provides relatively simple but precise methodology for edge detection problem, with the more demanding requirements on the

accuracy and robustness on the detection, the traditional algorithm can no longer handle the challenging edge detection task. The main defects of the traditional algorithm can be summarized as following:

1. Gaussian filter is applied to smooth out the noise, but it will also smooth the edge, which is considered as the high frequency feature. This will increase the possibility to miss weak edges, and the appearance of isolated edges in the result.

2. For the gradient amplitude calculation, the old canny edge detection algorithm uses center in a small 2*2 neighborhoods window to calculate the finite difference mean value to represent the gradient amplitude. This method is sensitive to noise and can easily detect fake edges and lose real edges.

3. In traditional canny edge detection algorithm, there will be two fixed global threshold values to filter out the false edges. However, as the image gets complex, different local areas will need very different threshold values to accurately find the real edges. In addition, the global threshold values are determined manually through experiments in the traditional method, which leads to complexity of calculation when large number of different images needs to be dealt with.

4. The result of the traditional detection cannot reach a satisfactory high accuracy of single response for each edge- multi-point responses will appear.

Parameters:

The Canny algorithm contains a number of adjustable parameters, which can affect the computation time and effectiveness of the algorithm.

1. The size of the Gaussian filter: the smoothing filter used in the first stage directly affects the results of the Canny algorithm. Smaller filters cause less blurring, and allow

detection of small, sharp lines. A larger filter causes more blurring, smearing out the value of a given pixel over a larger area of the image. Larger blurring radii are more useful for detecting larger, smoother edges – for instance, the edge of a rainbow.

2. Thresholds: the use of two thresholds with hysteresis allows more flexibility than in a single-threshold approach, but general problems of thresholding approaches still apply. A threshold set too high can miss important information. On the other hand, a threshold set too low will falsely identify irrelevant information (such as noise) as important. It is difficult to give a generic threshold that works well on all images. No tried and tested approach to this problem yet exists.

The Canny algorithm is adaptable to various environments. Its parameters allow it to be tailored to recognition of edges of differing characteristics depending on the particular requirements of a given implementation. In Canny's original paper, the derivation of the optimal filter led to a Finite Impulse Response filter, which can be slow to compute in the spatial domain if the amount of smoothing required is important (the filter will have a large spatial support in that case). For this reason, it is often suggested to use Rachid Deriche's infinite impulse response form of Canny's filter (the Canny–Deriche detector), which is recursive, and which can be computed in a short, fixed amount of time for any desired amount of smoothing. The second form is suitable for real time implementations in FPGAs or DSPs, or very fast embedded PCs. In this context, however, the regular recursive implementation of the Canny operator does not give a good approximation of rotational symmetry and therefore gives a bias towards horizontal and vertical edges.

3.2.4 Prewitt Edge Detector

The Prewitt operator is used in image processing, particularly within edge detection algorithms. Technically, it is a discrete differentiation operator, computing an

approximation of the gradient of the image intensity function. At each point in the image, the result of the Prewitt operator is either the corresponding gradient vector or the norm of this vector. The Prewitt operator is based on convolving the image with a small, separable, and integer valued filter in horizontal and vertical directions and is therefore relatively inexpensive in terms of computations. On the other hand, the gradient approximation which it produces is relatively crude, in particular for high frequency variations in the image. The Prewitt operator was developed by Judith M. S. Prewitt.

Mathematically, the operator uses two 3×3 kernels which are convolved with the original image to calculate approximations of the derivatives - one for horizontal changes, and one for vertical. If we define A as the source image, and G_x and G_y are two images which at each point contain the horizontal and vertical derivative approximations, the latter are computed as:

$$G_X = \begin{bmatrix} -1 & 0 & +1 \\ -1 & 0 & +1 \\ -1 & 0 & +1 \end{bmatrix} * A \ \ and \ \ G_Y = \begin{bmatrix} -1 & -1 & +1 \\ 0 & 0 & 0 \\ +1 & +1 & +1 \end{bmatrix} * A \qquad ----\rightarrow 8$$

where * here denotes the 2-dimensional convolution operation.

Since the Prewitt kernels can be decomposed as the products of an averaging and a differentiation kernel, they compute the gradient with smoothing. Therefore it is a separable filter. For example, G_x can be written as

$$\begin{bmatrix} -1 & 0 & +1 \\ -1 & 0 & +1 \\ -1 & 0 & +1 \end{bmatrix} = \begin{bmatrix} 1 \\ 1 \\ 1 \end{bmatrix} [-1 \quad 0 \quad 1] \qquad ----\rightarrow 9$$

The x-coordinate is defined here as increasing in the "right"-direction, and the y-coordinate is defined as increasing in the "down"-direction. At each point in the image,

the resulting gradient approximations can be combined to give the gradient magnitude, using:

$$G = \sqrt{G_x^2 + G_y^2} \qquad ----\rightarrow 10$$

Using this information, we can also calculate the gradient's direction:

$$\theta = atan2(G_y, G_x) \qquad ----\rightarrow 11$$

where, for example, Θ is 0 for a vertical edge which is darker on the right side.

Prewitt operator is used for edge detection in an image. It detects two types of edges:

1. Horizontal edges
2.VerticalEdges

Edges are calculated by using difference between corresponding pixel intensities of an image. All the masks that are used for edge detection are also known as derivative masks. Because as we have stated many times before in this series of tutorials that image is also a signal so changes in a signal can only be calculated using differentiation. So that's why these operators are also called as derivative operators or derivative masks.

All the derivative masks should have the following properties

1. Opposite sign should be present in the mask.
2. Sum of mask should be equal to zero.
3. More weight means more edge detection.

This mask will prominent the horizontal edges in an image. It also works on the principle of above mask and calculates difference among the pixel intensities of a particular edge. As the center row of mask is consist of zeros so it does not include the

original values of edge in the image but rather it calculate the difference of above and below pixel intensities of the particular edge. Thus increasing the sudden change of intensities and making the edge more visible. Both the above masks follow the principle of derivate mask. Both masks have opposite sign in them and both masks sum equals to zero. The third condition will not be applicable in this operator as both the above masks are standardize and we can't change the value in them.

3.2.5 SURF

SURF is a detector and a high-performance descriptor points of interest in an image where the image is transformed into coordinates, using a technique called multi-resolution. Is to make a copy of the original image with Pyramidal Gaussian or Laplacian Pyramid shape and obtain image with the same size but with reduced bandwidth. Thus a special blurring effect on the original image, called Scale-Space is achieved. This technique ensures that the points of interest are scale invariant. The SURF algorithm is based on the SIFT predecessor.

Scale-space representation & location of points of interest

The attractions can be found in different scales, partly because the search for correspondences often requires comparison images where they are seen at different scales. The scale spaces are generally applied as a pyramid image . Images are repeatedly smoothed with a Gaussian filter, then, is sub sampled to achieve a higher level of the pyramid. Therefore, several floors or stairs " det H" with various measures of the masks are calculated.

The scale -space is divided into a number of octaves, Where an octave refers to a series of response maps of covering a doubling of scale . In SURF The Lowest level of the Scale- space is Obtained from the output of the 9 × 9 filters.

Scale spaces are implemented by applying box filters of different size. Therefore, the scale space is analyzed by up-scaling the filter size rather than iteratively reducing the image size. The output of the above 9*9 filter is considered as the initial scale layer, to which we will refer as scale s=1.2 (corresponding to Gaussian derivatives with σ=1.2). The following layers are obtained by filtering the image with gradually bigger masks, taking into account the discrete nature of integral images and the specific structure of or filters. Specifically, this results in filters of size 9*9, 15*15, 21*21, 27*27, etc. In order to localize interest points in the image and over scales, non-maximum suppression in a 3*3*3 neighborhood is applied. The maxima of the determinant of the Hessian matrix are then interpolated in scale and image space with the method proposed by Brown et al. Scale space interpolation is especially important in our case, as the difference in scale between the first layers of every octave is relatively large.

After 3D maxima are looking at (x, y, n) using the cube 3x3x3 neighborhood . From there it is proceed to do the interpolation of the maximum. Lowe rest of the layers of the pyramid to get the DOG (Difference of Gaussian) find images contours and stains.

Specifically, it is entered by variant a quick and Van Gool Neubecker used. The maximum of the determinant of the Hessian matrix in scale and space interpolated image with Brown and Lowe proposed method. The approach of the determinant of the Hessian matrix represents the response of BLOB in the image to the location x. These responses are stored in the BLOB map of responses on different scales. They have the principal feature of repetibility, That means if some point is considered realiable, the detector will find the same point under different perspective (scale, orientation, rotation, etc.).

It has one position (x,y) for each interest point.

Description:

The goal of a descriptor is to provide a unique and robust description of an image feature, e.g. by describing the intensity distribution of the pixels within the neighborhood of the point of interest. Most descriptors are computed thus in a local manner; hence, a description is obtained for every point of interest identified previously.

The dimensionality of the descriptor has direct impact on both its computational complexity and point-matching robustness/accuracy. A short descriptor may be more robust against appearance variations, but may not offer sufficient discrimination and thus give too many false positives.

The next three introducing steps are explained in the following: The first step consists of fixing a reproducible orientation based on information from a circular region around the interest point. Then, we construct a square region aligned to the selected orientation and extract the SURF descriptor from it. Finally, features are matched between two images.

The SURF descriptor is based on the similar properties of SIFT, with a complexity stripped down even further. The first step consists of fixing a reproducible orientation based on information from a circular region around the interest point. The second step is constructing as square region aligned to the selected orientation, and extracting the SURF descriptor from it. These two steps are now explained in turn. Furthermore, we also propose an upright version of our descriptor (U-SURF) that is not invariant to image rotation and therefore faster to compute and better suited for application where the camera remains more or less horizontal.

Matching

This section details the step back in search of characteristic points that provides the detector. This way it is possible to compare between descriptors and look for matching pairs of images between them. There are two ways to do it:

1. Get the characteristic points of the first image and its descriptor and do the same with the second image . So you will be able to compare the two images descriptor correspondences between points and establish some kind of measure.

2. Get the characteristic points of the first image with the descriptor. Then compare this descriptor with the points of the second image which is believed to be the partner concerned.

3.2.6 SIFT:

Scale-invariant feature transform (or SIFT) is an algorithm in computer vision to detect and describe local features in images. Applications include object recognition, robotic mapping and navigation, image stitching, 3D modeling, gesture recognition, video tracking, individual identification of wildlife and match moving.

For any object in an image, interesting points on the object can be extracted to provide a "feature description" of the object. This description, extracted from a training image, can then be used to identify the object when attempting to locate the object in a test image containing many other objects. To perform reliable recognition, it is important that the features extracted from the training image be detectable even under changes in image scale, noise and illumination. Such points usually lie on high-contrast regions of the image, such as object edges.

Another important characteristic of these features is that the relative positions between them in the original scene shouldn't change from one image to another. For

example, if only the four corners of a door were used as features, they would work regardless of the door's position; but if points in the frame were also used, the recognition would fail if the door is opened or closed. Similarly, features located in articulated or flexible objects would typically not work if any change in their internal geometry happens between two images in the set being processed. However, in practice SIFT detects and uses a much larger number of features from the images, which reduces the contribution of the errors caused by these local variations in the average error of all feature matching errors.

SIFT can robustly identify objects even among clutter and under partial occlusion, because the SIFT feature descriptor is invariant to uniform scaling, orientation, and partially invariant to affine distortion and illumination changes. This section summarizes Lowe's object recognition method and mentions a few competing techniques available for object recognition under clutter and partial occlusion

SIFT key points of objects are first extracted from a set of reference images and stored in a database. An object is recognized in a new image by individually comparing each feature from the new image to this database and finding candidate matching features based on Euclidean distance of their feature vectors. From the full set of matches, subsets of keypoints that agree on the object and its location, scale, and orientation in the new image are identified to filter out good matches. The determination of consistent clusters is performed rapidly by using an efficient hash table implementation of the generalized Hough transform. Each cluster of 3 or more features that agree on an object and its pose is then subject to further detailed model verification and subsequently outliers are discarded. Finally the probability that a particular set of features indicates the presence of an object is computed, given the accuracy of fit and number of probable false matches. Object matches that pass all these tests can be identified as correct with high confidence.

Features:

The detection and description of local image features can help in object recognition. The SIFT features are local and based on the appearance of the object at particular interest points, and are invariant to image scale and rotation. They are also robust to changes in illumination, noise, and minor changes in viewpoint. In addition to these properties, they are highly distinctive, relatively easy to extract and allow for correct object identification with low probability of mismatch. They are relatively easy to match against a (large) database of local features but however the high dimensionality can be an issue, and generally probabilistic algorithms such as k-d trees with best bin first search are used. Object description by set of SIFT features is also robust to partial occlusion; as few as 3 SIFT features from an object are enough to compute its location and pose. Recognition can be performed in close-to-real time, at least for small databases and on modern computer hardware

Scale-invariant feature detection:

Lowe's method for image feature generation transforms an image into a large collection of feature vectors, each of which is invariant to image translation, scaling, and rotation, partially invariant to illumination changes and robust to local geometric distortion. These features share similar properties with neurons in inferior temporal cortex that are used for object recognition in primate vision. Key locations are defined as maxima and minima of the result of difference of Gaussians function applied in scale space to a series of smoothed and resampled images. Low contrast candidate points and edge response points along an edge are discarded. Dominant orientations are assigned to localized keypoints. These steps ensure that the keypoints are more stable for matching and recognition. SIFT descriptors robust to local affine distortion are then obtained by

considering pixels around a radius of the key location, blurring and resampling of local image orientation planes

Feature matching and indexing:

Indexing consists of storing SIFT keys and identifying matching keys from the new image. Lowe used a modification of the k-d tree algorithm called the Best-bin-first search method that can identify the nearest neighbors with high probability using only a limited amount of computation. The BBF algorithm uses a modified search ordering for the k-d tree algorithm so that bins in feature space are searched in the order of their closest distance from the query location. This search order requires the use of a heap-based priority queue for efficient determination of the search order. The best candidate match for each keypoint is found by identifying its nearest neighbor in the database of keypoints from training images. The nearest neighbors are defined as the keypoints with minimum Euclidean distance from the given descriptor vector. The probability that a match is correct can be determined by taking the ratio of distance from the closest neighbor to the distance of the second closest.

Lower rejected all matches in which the distance ratio is greater than 0.8, which eliminates 90% of the false matches while discarding less than 5% of the correct matches. To further improve the efficiency of the best-bin-first algorithm search was cut off after checking the first 200 nearest neighbor candidates. For a database of 100,000 keypoints, this provides a speedup over exact nearest neighbor search by about 2 orders of magnitude, yet results in less than a 5% loss in the number of correct matches.

Cluster identification by Hough transform voting:

Hough Transform is used to cluster reliable model hypotheses to search for keys that agree upon a particular model pose. Hough transform identifies clusters of features with a consistent interpretation by using each feature to vote for all object poses that are

consistent with the feature. When clusters of features are found to vote for the same pose of an object, the probability of the interpretation being correct is much higher than for any single feature. An entry in a hash table is created predicting the model location, orientation, and scale from the match hypothesis.The hash table is searched to identify all clusters of at least 3 entries in a bin, and the bins are sorted into decreasing order of size.

Each of the SIFT keypoints specifies 2D location, scale, and orientation, and each matched keypoint in the database has a record of its parameters relative to the training image in which it was found. The similarity transform implied by these 4 parameters is only an approximation to the full 6 degree-of-freedom pose space for a 3D object and also does not account for any non-rigid deformations. Therefore, Lower used broad bin sizes of 30 degrees for orientation, a factor of 2 for scale, and 0.25 times the maximum projected training image dimension (using the predicted scale) for location. The SIFT key samples generated at the larger scale are given twice the weight of those at the smaller scale. This means that the larger scale is in effect able to filter the most likely neighbours for checking at the smaller scale. This also improves recognition performance by giving more weight to the least-noisy scale. To avoid the problem of boundary effects in bin assignment, each keypoint match votes for the 2 closest bins in each dimension, giving a total of 16 entries for each hypothesis and further broadening the pose range.

Model verification by linear least squares:

Each identified cluster is then subject to a verification procedure in which a linear least squares solution is performed for the parameters of the affine transformation relating the model to the image. The affine transformation of a model point [x y]_T to an image point [u v]_T can be written as below

$$\begin{bmatrix} u \\ v \end{bmatrix} = \begin{bmatrix} m1 & m2 \\ m3 & m4 \end{bmatrix} \begin{bmatrix} x \\ y \end{bmatrix} + \begin{bmatrix} tx \\ ty \end{bmatrix} \qquad ----\rightarrow 12$$

where the model translation is [tx ty]T and the affine rotation, scale, and stretch are represented by the parameters m1, m2, m3 and m4. To solve for the transformation parameters the equation above can be rewritten to gather the unknowns into a column vector.

$$\begin{bmatrix} x & y & 0 & 0 & 1 & 0 \\ 0 & 0 & x & y & 0 & 1 \\ . & & & & & \\ . & & & & & \\ . & & & & & \end{bmatrix} \begin{bmatrix} m1 \\ m2 \\ m3 \\ m4 \\ tx \\ ty \end{bmatrix} = \begin{bmatrix} u \\ v \\ . \\ . \end{bmatrix} \qquad -----13$$

This equation shows a single match, but any number of further matches can be added, with each match contributing two more rows to the first and last matrix. At least 3 matches are needed to provide a solution. We can write this linear system as

$$A\hat{x} \approx b, \qquad ----\rightarrow 14$$

where A is a known m-by-n matrix (usually with m > n), x is an unknown n-dimensional parameter vector, and b is a known m-dimensional measurement vector.

Therefore the minimizing vector is a solution of the normal equation

$$A^T A\hat{x} = A^T b \qquad ----\rightarrow 15$$

The solution of the system of linear equations is given in terms of the matrix, called the pseudoinverse of A, by

$$\hat{x} = (A^T A)^{-1} A^T b - - - - \rightarrow 16$$

Which minimizes the sum of the squares of the distances from the projected model locations to the corresponding image locations.

Outlier detection:

Outliers can now be removed by checking for agreement between each image feature and the model, given the parameter solution. Given the linear least squares solution, each match is required to agree within half the error range that was used for the parameters in the Hough transform bins. As outliers are discarded, the linear least squares solution is re-solved with the remaining points, and the process iterated. If fewer than 3 points remain after discarding outliers, then the match is rejected. In addition, a top-down matching phase is used to add any further matches that agree with the projected model position, which may have been missed from the Hough transform bin due to the similarity transform approximation or other errors.

The final decision to accept or reject a model hypothesis is based on a detailed probabilistic model. This method first computes the expected number of false matches to the model pose, given the projected size of the model, the number of features within the region, and the accuracy of the fit. A Bayesian probability analysis then gives the probability that the object is present based on the actual number of matching features found. A model is accepted if the final probability for a correct interpretation is greater than 0.98. Lowe's SIFT based object recognition gives excellent results except under wide illumination variations and under non-rigid transformations.

3.2.7 Comparison:

There has been an extensive study done on the performance evaluation of different local descriptors, including SIFT, using a range of detectors. The main results are summarized below:

SIFT and SIFT-like GLOH features exhibit the highest matching accuracies (recall rates) for an affine transformation of 50 degrees. After this transformation limit, results start to become unreliable.

Distinctiveness of descriptors is measured by summing the eigenvalues of the descriptors, obtained by the Principal components analysis of the descriptors normalized by their variance. This corresponds to the amount of variance captured by different descriptors, therefore, to their distinctiveness. PCA-SIFT (Principal Components Analysis applied to SIFT descriptors), GLOH and SIFT features give the highest values.
SIFT-based descriptors outperform other contemporary local descriptors on both textured and structured scenes, with the difference in performance larger on the textured scene.
For scale changes in the range 2-2.5 and image rotations in the range 30 to 45 degrees, SIFT and SIFT-based descriptors again outperform other contemporary local descriptors with both textured and structured scene content.

Introduction of blur affects all local descriptors, especially those based on edges, like shape context, because edges disappear in the case of a strong blur. But GLOH, PCA-SIFT and SIFT still performed better than the others. This is also true for evaluation in the case of illumination changes.

The evaluations carried out suggests strongly that SIFT-based descriptors, which are region-based, are the most robust and distinctive, and are therefore best suited for feature matching. However, most recent feature descriptors such as SURF have not been evaluated in this study.

SURF has later been shown to have similar performance to SIFT, while at the same time being much faster. Another study concludes that when speed is not critical, SIFT outperforms SURF.

Recently, a slight variation of the descriptor employing an irregular histogram grid has been proposed that significantly improves its performance. Instead of using a 4x4 grid of histogram bins, all bins extend to the center of the feature. This improves the descriptor's robustness to scale changes.

The SIFT-Rank descriptor was shown to improve the performance of the standard SIFT descriptor for affine feature matching. A SIFT-Rank descriptor is generated from a standard SIFT descriptor, by setting each histogram bin to its rank in a sorted array of bins. The Euclidean distance between SIFT-Rank descriptors is invariant to arbitrary monotonic changes in histogram bin values, and is related to Spearman's rank correlation coefficient.

Object recognition using SIFT features:

Given SIFT's ability to find distinctive keypoints that are invariant to location, scale and rotation, and robust to affine transformations (changes in scale, rotation, shear, and position) and changes in illumination, they are usable for object recognition. The steps are given below.

First, SIFT features are obtained from the input image using the algorithm described above.

These features are matched to the SIFT feature database obtained from the training images. This feature matching is done through a Euclidean-distance based nearest

neighbor approach. To increase robustness, matches are rejected for those keypoints for which the ratio of the nearest neighbor distance to the second nearest neighbor distance is greater than 0.8. This discards many of the false matches arising from background clutter. Finally, to avoid the expensive search required for finding the Euclidean-distance-based nearest neighbor, an approximate algorithm called the best-bin-first algorithm is used. This is a fast method for returning the nearest neighbor with high probability, and can give speedup by factor of 1000 while finding nearest neighbor (of interest) 95% of the time.

Although the distance ratio test described above discards many of the false matches arising from background clutter, we still have matches that belong to different objects. Therefore to increase robustness to object identification, we want to cluster those features that belong to the same object and reject the matches that are left out in the clustering process. This is done using the Hough transform. This will identify clusters of features that vote for the same object pose. When clusters of features are found to vote for the same pose of an object, the probability of the interpretation being correct is much higher than for any single feature. Each keypoint votes for the set of object poses that are consistent with the keypoint's location, scale, and orientation. Bins that accumulate at least 3 votes are identified as candidate object/pose matches.

For each candidate cluster, a least-squares solution for the best estimated affine projection parameters relating the training image to the input image is obtained. If the projection of a keypoint through these parameters lies within half the error range that was used for the parameters in the Hough transform bins, the keypoint match is kept. If fewer than 3 points remain after discarding outliers for a bin, then the object match is rejected. The least-squares fitting is repeated until no more rejections take place. This works better for planar surface recognition than 3D object recognition since the affine model is no longer accurate for 3D objects.

In this journal, authors proposed a new approach to use SIFT descriptors for multiple object detection purposes. The proposed multiple object detection approach is tested on aerial and satellite images.

SIFT features can essentially be applied to any task that requires identification of matching locations between images. Work has been done on applications such as recognition of particular object categories in 2D images, 3D reconstruction, motion tracking and segmentation, robot localization, image panorama stitching and epipolar calibration. Some of these are discussed in more detail below.

3D SIFT-like descriptors for human action recognition:

Extensions of the SIFT descriptor to 2+1-dimensional spatio-temporal data in context of human action recognition in video sequences have been studied. The computation of local position-dependent histograms in the 2D SIFT algorithm are extended from two to three dimensions to describe SIFT features in a spatio-temporal domain. For application to human action recognition in a video sequence, sampling of the training videos is carried out either at spatio-temporal interest points or at randomly determined locations, times and scales. The spatio-temporal regions around these interest points are then described using the 3D SIFT descriptor. These descriptors are then clustered to form a spatio-temporal Bag of words model. 3D SIFT descriptors extracted from the test videos are then matched against these words for human action classification.

The authors report much better results with their 3D SIFT descriptor approach than with other approaches like simple 2D SIFT descriptors and Gradient Magnitude.

CHAPTER 4

RESULT AND DISCUSSSIONS

4.1 Output of Canny Operator:

Fig.4.1 Original image

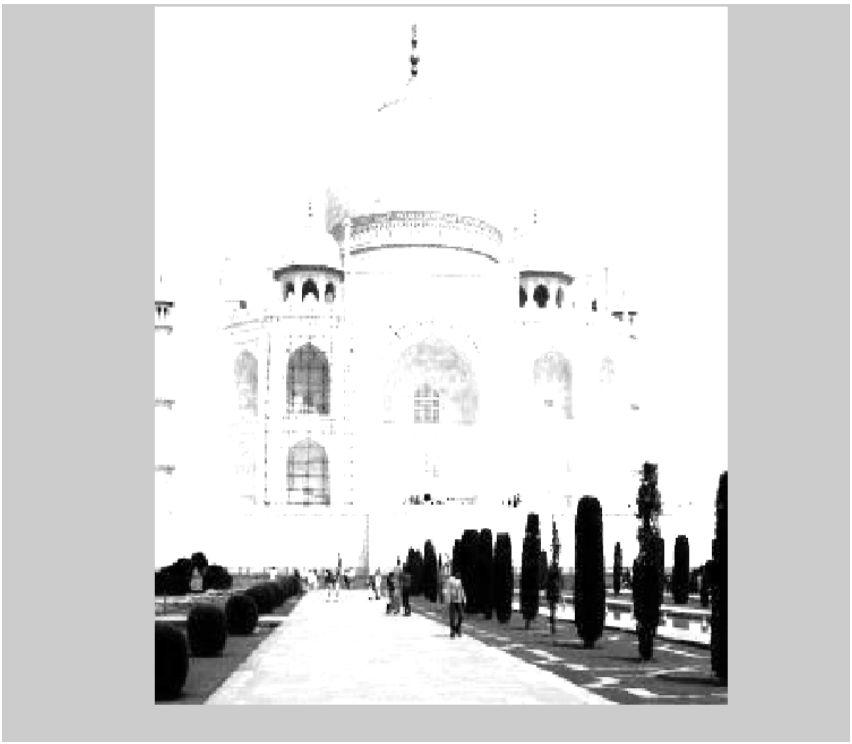

Fig.4.2 Filtered Image

Fig.4.3 Canny Edge Detector

4.2 Output of Sobel Operator:

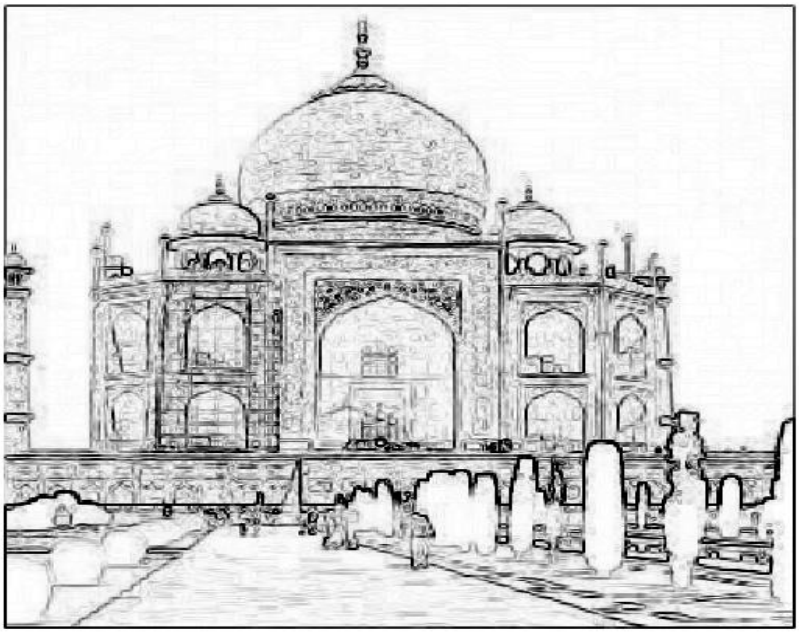

Fig.4.4Sobel Edge Detector

4.3 Output of Prewitt Operator:

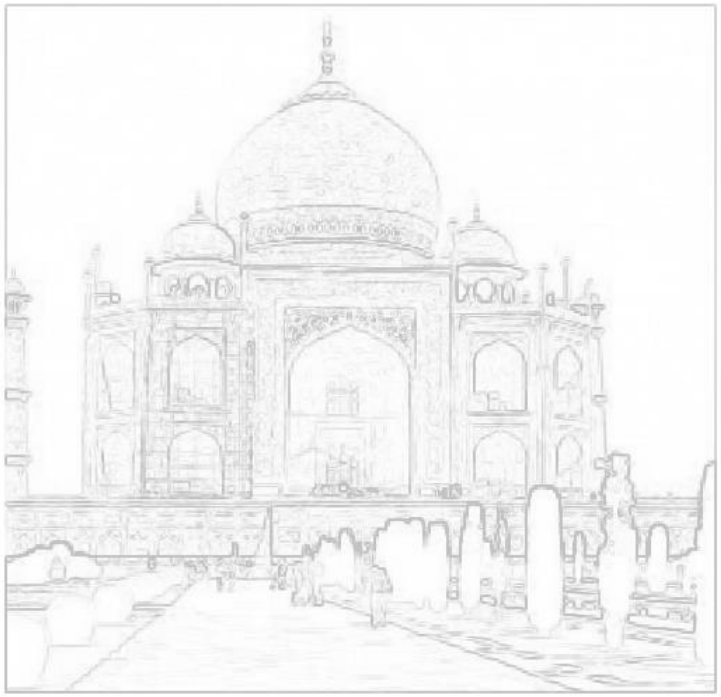

Fig.4.5Prewitt Edge Detector

4.4 Output of SIFT Edge Detection Images:

Fig.4.6 Edges

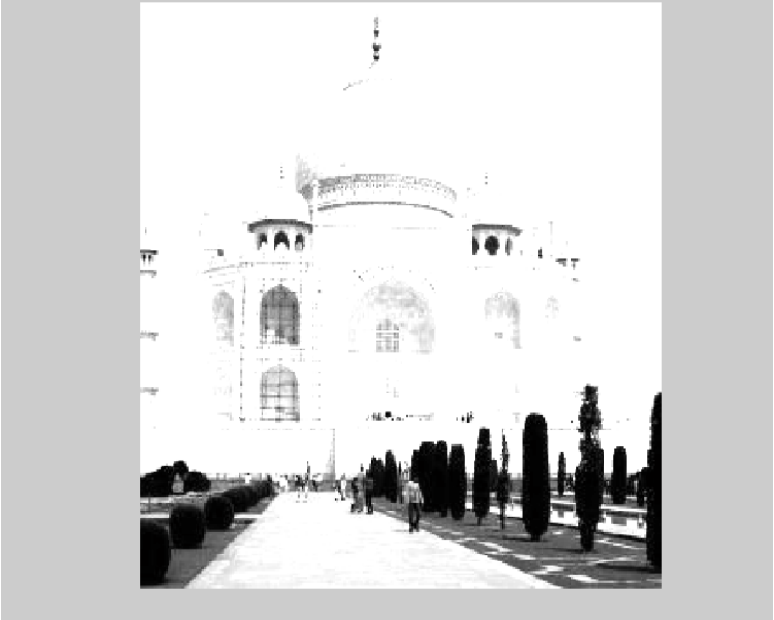

Fig.4.7 Decrease Intensity

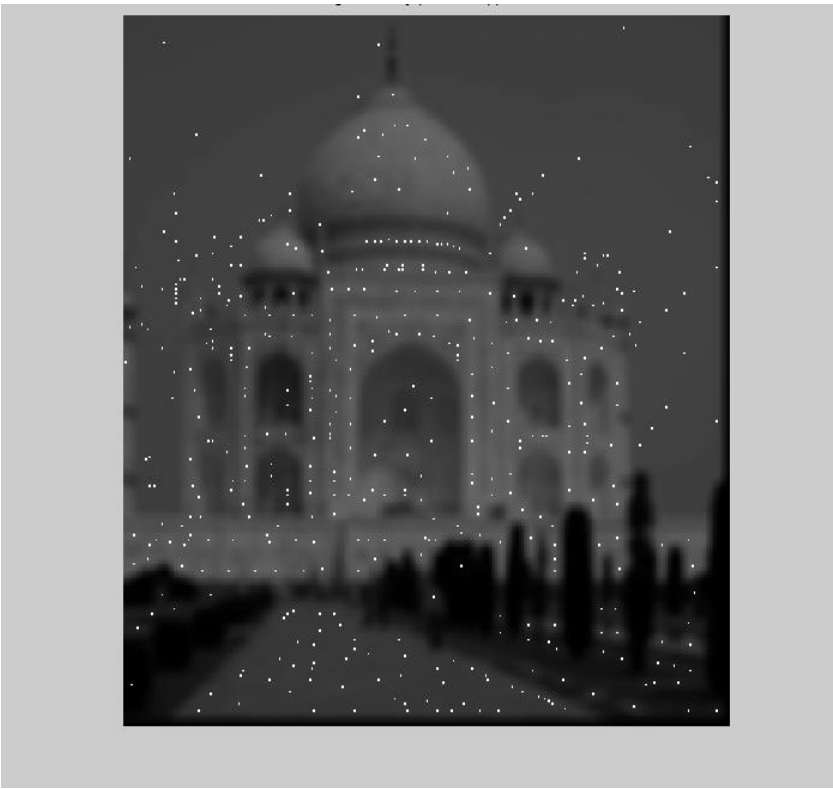

Fig.4.8 Decrease Intensity Edges

Fig.4.9 Increase Intensity

Fig.4.10 Increase Intensity Edges

Fig.4.11 Rotated Image

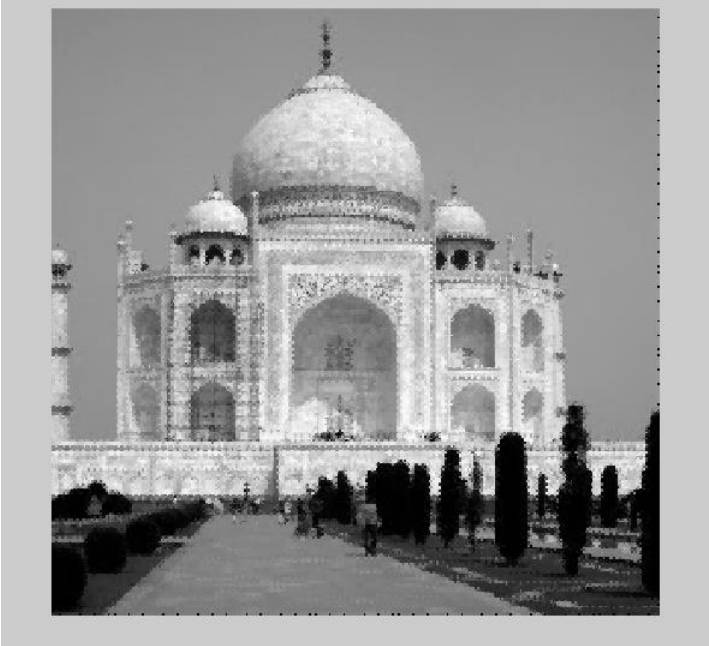

Fig.4.12 Rotate Comparison

Fig.4.13 Rotated Edges

4.5 OUTPUT OF SURF:

Fig.4.14 SURF OUTPUT

CHAPTER 5

CONCLUSION

5.1 Comparison of SURF Output and SIFT Output

Two feature detection methods for image registration. Based on the experimental results, it is found that the SIFT has detected more number of features compared to SURF but it is suffered with speed. The SURF is fast and has good performance as the same as SIFT.

Table.5.1.1 COMPARISON TABLE

ALGORITHM	MATCHING FEATURES	FEATURES MATCHING TIME
SIFT	13	1.543s
SURF	6	0.564s

REFERENCES

1. Myung Jin Choi, Antonio Torralba and Alan S. Willsky, “A Tree-Based Context Model for Object Recognition,” IEEE Trans. Pattern Analysis and Machine Intelligence, vol. 34

2. N. Dalal and B. Triggs, “Histograms of Oriented Gradients for Human Detection,” Proc. IEEE CS Conf. Computer Vision and Pattern Recognition, 2005.

3. J. Deng, W. Dong, R. Socher, L.-J. Li, K. Li, and L. Fei-Fei, “ImageNet: A Large-Scale Hierarchical Image Database,” Proc. IEEE Conf. Computer Vision and Pattern Recognition, 2009.

4. S.K. Divvala, D. Hoiem, J.H. Hays, A.A. Efros, and M. Hebert, “An Empirical Study of Context in Object Detection,” Proc. IEEE Conf. Computer Vision and Pattern Recognition, 2009.

5. M. Everingham, L. Van Gool, C.K.I. Williams, J. Winn, and A.Zisserman, “The PASCAL Visual Object Classes Challenge 2007 (VOC2007) Results,” , 2011.

6. P. Felzenszwalb, R. Girshick, D. McAllester, and D. Ramanan, “Object Detection with Discriminatively Trained Part Based Models,” IEEE Trans. Pattern Analysis and Machine Intelligence, vol. 32, no. 9, pp. 1627-1645, Sept. 2010.

7. R. Fergus, P. Perona, and A. Zisserman, “Object Class Recognition by Unsupervised Scale-Invariant Learning,” Proc. IEEE CS Conf. Computer Vision and Pattern Recognition, 2003.

8. C. Galleguillos, A. Rabinovich, and S. Belongie, “Object Categorization Using Co-Occurrence, Location and Appearance,” Proc. IEEE Conf. Computer Vision and Pattern Recognition, 2008.

9. S. Gould, J. Rodgers, D. Cohen, G. Elidan, and D. Koller, “Multi- Class Segmentation with Relative Location Prior,” Int’l J. Computer Vision, vol. 80, pp. 300-316, 2007.

10. X. He, R.S. Zemel, and M._ A. Carreira-Perpinn˜a´n, “Multiscale Conditional Random Fields for Image Labeling,” Proc. IEEE CS Conf. Computer Vision and Pattern Recognition, 2004.

11. G. Heitz, S. Gould, A. Saxena, and D. Koller, “Cascaded Classification Models: Combining Models for Holistic Scene Understanding,” Proc. Neural Information Processing Systems, 2008.

12. D. Hoiem, A. Efros, and M. Hebert, “Putting Objects in Perspective,” Proc. IEEE CS Conf. Computer Vision and Pattern Recognition, 2006.

13. Y. Jin and S. Geman, “Context and Hierarchy in a Probabilistic Image Model,” Proc. IEEE CS Conf. Computer Vision and Pattern Recognition, 2006.

14. L.-J. Li, R. Socher, and L. Fei-Fei, “Towards Total Scene Understanding: Classification, Annotation and Segmentation in an Automatic Framework,” Proc. IEEE Conf. Computer Vision and Pattern Recognition, 2009.

15. M. Marszałek and C. Schmid, “Semantic Hierarchies for Visual Object Recognition,” Proc. IEEE Conf. Computer Vision and Pattern Recognition, 2007.

16. J. Porway, K. Wang, B. Yao, and S.C. Zhu, “A Hierarchical and Contextual Model for Aerial Image Understanding,” Proc. IEEE Conf. Computer Vision and Pattern Recognition, 2008.

17. Z. Tu, “Auto-Context and Its Application to High-Level Vision Tasks,” Proc. IEEE Conf. Computer Vision and Pattern Recognition, 2008.

Aravindh A.S., B.Tech.
asaravindh.121193@gmail.com

J. Christy Samuel

==========
Engineering & Technology in India www.engineeringandtechnologyinindia.com
Vol. 1:2 March 2016
==========

Application Level Semantics for Compressing Group Movement Patterns in Wireless Sensor Networks

J. Biju, M.E.

==========

Abstract

This paper proposes an efficient distributed mining algorithm to jointly identify a group of moving objects and discover their movement patterns in wireless sensor networks. Then propose a compression algorithm, called two–phase and two-dimensional algorithm, which exploits the obtained group movement patterns to reduce the amount of delivered data. The compression algorithm includes a sequence merge phase and an entropy reduction phase. In the sequence merge phase, propose a merge algorithm to merge and compress the location data of a group of moving objects. In the entropy reduction phase, formulate a Hit Item Replacement (HIR) problem and propose a replace algorithm that obtains the optimal solution. Then devise three replacement rules and derive the maximum compression ratio. The experimental results show that the proposed compression algorithm leverages the group movement patterns to reduce the amount of delivered data effectively and efficiently.

Key words: mining algorithm, wireless sensor, compression leverages

1. Introduction

Recent advances in location-acquisition technologies, such as global positioning systems (GPSs) and wireless sensor networks (WSNs), have fostered many novel applications like object tracking, environmental monitoring, and location-dependent service. These applications generate a large amount of location data, and thus, lead to transmission and storage challenges, especially

in resource constrained environments like WSNs. To reduce the data volume, various algorithms have been proposed for data compression and data aggregation.

However, the above works do not address application-level semantics, such as the group relationships and movement patterns, in the location data. In object tracking applications, many natural phenomena show that objects often exhibit some degree of regularity in their movements.

Discovering the group movement patterns is more difficult than finding the patterns of a single object or all objects, because we need to jointly identify a group of objects and discover their aggregated group movement patterns. However, few of existing approaches consider these issues simultaneously. On the one hand, the temporal-and-spatial correlations in the movements of moving objects are modeled as sequential patterns in data mining to discover the frequent movement patterns we first introduce our distributed mining algorithm to approach the moving object clustering problem and discover group movement patterns. Then, based on the discovered group movement patterns, we propose a novel compression algorithm to tackle the group data compression problem.

Our distributed mining algorithm comprises a Group Movement Pattern Mining (GMPMine) and Cluster Ensembling (CE) algorithms. It avoids transmitting unnecessary and redundant data by transmitting only the local grouping results to a base station (the sink), instead of all of the moving objects' location data. Specifically, the GMP Mine algorithm discovers the local group movement patterns by using a novel similarity measure, while the CE algorithm combines the local grouping results.

To remove inconsistency and improve the grouping quality by using the information theory, the constrained resource of WSNs should also be considered in approaching the moving object clustering problem.

This is different from previous works. We formulate a moving object clustering problem that jointly identifies a group of objects and discovers their movement patterns. The application-level semantics are useful for various applications, such as data storage and transmission, task scheduling, and network construction.

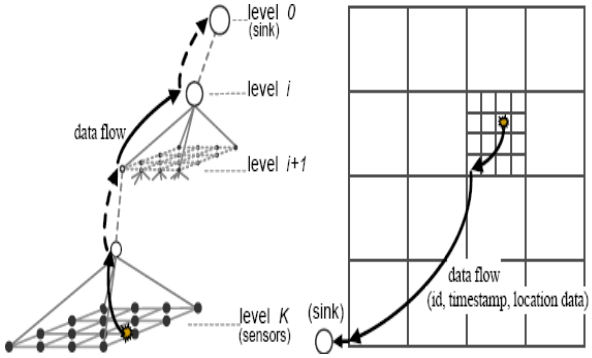

Figure 1.1: Network and location models

2. Proposed Compression Method

Consider the pattern projection method in mining sequential patterns and proposed FreeSpan, which is an FP-growth-based algorithm. Yang and Hu developed a new match measure for imprecise trajectory data and proposed Traj Pattern to mine sequential patterns. Many variations derived from sequential patterns are used in various applications, e.g., Chen et al. discover path traversal patterns in a Web environment, while Peng and Chen mine user moving patterns incrementally in a mobile computing system. However, sequential patterns and its variations do not provide sufficient information for location prediction or clustering. First, they carry no time information between consecutive items, so they cannot provide accurate information for location prediction when time is concerned. Second, they consider the characteristics of all objects, which make the meaningful movement characteristics of individual objects or a group of moving objects inconspicuous and ignored. Third, because a sequential pattern lacks information about its significance regarding to each individual trajectory, they are not fully representative to individual trajectories.

To discover significant patterns for location prediction, Morzy mines frequent trajectories whose consecutive items are also adjacent in the original trajectory data. Meanwhile, Giannotti, et al. extract T-patterns from spatiotemporal data sets to provide concise descriptions of frequent movements, and Tseng and Lin proposed the GMP Mine algorithm for discovering the temporal movement patterns. However, the above A priori-like or FP-growth based algorithms still focus

on discovering frequent patterns of all objects and may suffer from computing efficiency or memory problems, which make them unsuitable for use in resource-constrained environments.

For each of their significant movement patterns, the new similarity measure considers not merely two probability distributions but also two weight factors.

The similarity score simp. of oi and oj based on their respective PSTs, Ti and Tj, is defined as follows**:**

$$sim_p = -log \frac{\sum_{s \in \tilde{S}} \sqrt{\sum_{\sigma \in \Sigma} \left(P^{T_1}(s\sigma) - P^{T_2}(s\sigma) \right)^2}}{2L_{max} + \sqrt{2}}$$

The similarity score simp includes the distance associated with a pattern s, defined as,

$$d(s) = \sqrt{\sum_{\sigma \in \Sigma} \left(P^{T_i}(s\sigma) - P^{T_j}(s\sigma) \right)^2}$$
$$= \sqrt{\sum_{\sigma \in \Sigma} \left(P^{T_i}(s) \times P^{T_i}(\sigma|s) - P^{T_j}(s) \times P^{T_j}(\sigma|s) \right)^2},$$

where d(s) is the Euclidean distance associated with a pattern s over Ti and Tj.

A. Clustering

Recently, clustering based on objects' movement behavior has attracted more attention. Wang et al. transform the location sequences into a transaction-like data on users and based on which to obtain a valid group, but the proposed AGP and VG growth are still A priori-like or FP-growth based algorithms that suffer from high computing cost and memory demand. Nanni and Pedreschi proposed a density-based clustering algorithm, which makes use of an optimal time interval and the average Euclidean distance between each point of two trajectories, to approach the trajectory clustering problem. However, the above works discover global group relationships based on the proportion of the time a group of users stay close together to the whole time duration or the average Euclidean distance of the entire trajectories.

Thus, they may not be able to reveal the local group relationships, which are required for many applications. In addition, though computing the average Euclidean distance of two geometric trajectories is simple and useful, the geometric coordinates are expensive and not always available. Approaches, such as EDR, LCSS, and DTW, are widely used to compute the similarity of symbolic trajectory sequences , but the above dynamic programming approaches suffer from scalability problem . To provide scalability, approximation or summarization techniques are used to represent original data. Guralnik and Karypis project each sequence into a vector space of sequential patterns and use a vector-based K-means algorithm to cluster objects.

However, the importance of a sequential pattern regarding individual sequences can be very different, which is not considered in this work. To cluster sequences, Yang and Wang proposed CLUSEQ, which iteratively identifies a sequence to a learned model, yet the generated clusters may overlap which differentiates their problem from ours.

B. Data Compression

Data compression can reduce the storage and energy consumption for resource-constrained applications. In distributed source (Slepian-Wolf) coding uses joint entropy to encode two nodes' data individually without sharing any data between them; however, it requires prior knowledge of cross correlations of sources. Other works include such as combine data compression with routing by exploiting cross correlations between sensor nodes to reduce the data size. In a tailed LZW has been proposed to address the memory constraint of a sensor device. Summarization of the original data by regression or linear modeling has been proposed for trajectory data compression. However, the above works do not address application-level semantics in data, such as the correlations of a group of moving objects, which we exploit to enhance the compressibility.

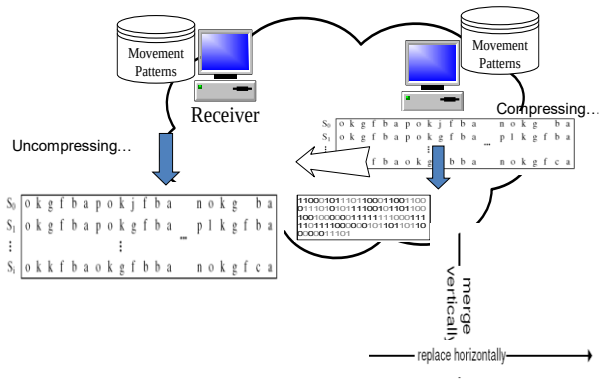

Figure 1.5 Design of a Compression Algorithm

C. Sequence Merge Phase

In the application of tracking wild animals, multiple moving objects may have group relationships and share similar trajectories. In this case, transmitting their location data separately leads to redundancy. Therefore, in this section, we concentrate on the problem of compressing multiple similar sequences of a group of moving objects.

D. Entropy Reduction Phase

In the entropy reduction phase, we propose the Replace algorithm to minimize the entropy of the merged sequence obtained in the sequence merge phase. Since data with lower entropy require fewer bits for storage and transmission, we replace some items to reduce the entropy without loss of information. The object movement patterns discovered by our distributed mining algorithm enable us to find the replaceable items and facilitate the selection of items in our compression algorithm. In this section, we first introduce and define the HIR problem, and then, explore the properties of Shannon's entropy to solve the HIR problem. We extend the concentration property for entropy reduction and discuss the benefits of replacing multiple symbols simultaneously. We derive three replacement rules for the HIR problem and prove that the entropy of the obtained solution is minimized.

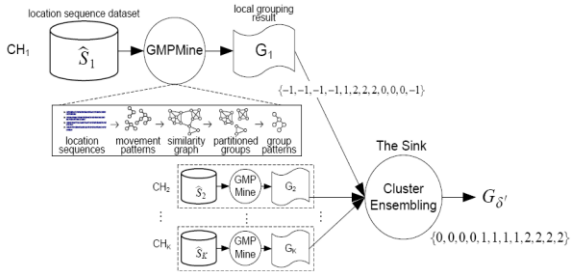

Figure3.2:Group movement pattern mining algorithm

E. Segmentation, Alignment, and Packaging

In an online update approach, sensor nodes are assigned a tracking task to update the sink with the location of moving objects at every tracking interval. In contrast to the online approach, the CHs in our batch-based approach accumulate a large volume of location data for a batch period before compressing and transmitting it to the sink; and the location update process repeats from batch to batch. In real-world tracking scenarios, slight irregularities of the movements of a group of moving objects may exist in the microcosmic view. Specifically, a group of objects may enter a sensor cluster at slightly different times and stay in a sensor cluster for slightly different periods, which lead to the alignment problem among the location sequences. Moreover, since the trajectories of moving objects may span multiple sensor clusters, and the objects may enter and leave a cluster. multiple times during a batch period, a location sequence may comprise multiple segments, each of which is a trajectory that is continuous in time domain. To deal with the alignment and segmentation problems, we partition location sequences into segments, and then, compress and package them into one update packet

3. Conclusion

The compression algorithm effectively reduces the amount of delivered data and enhances compressibility by extension, reduces the energy consumption expense for data transmission in Wireless Sensor Networks by exploiting the characteristics of group movement patterns to discover the information about groups of moving objects in tracking applications. The distributed mining algorithm consists of a local GMP Mine algorithm and a CE Algorithm to discover the group movement patterns.

With the discovered information ,devise the Two-Phase and Two–Dimensional algorithm ,which comprises a sequence merge phase and an entropy reduction phase. In sequence merge phase, propose the merge algorithm to merge the location sequences of a group of moving objects with the goal of reducing the overall sequence length. In the entropy reduction phase formulate the HIR problem and propose a replace algorithm to tackle the HIR problem. In addition devise and prove three replacement rules, with which the Replace algorithm obtains the optimal solution of HIR effectively.

==========

References

[1] Hsiao-Ping Tsai,IEEE,De-Nian Yang,and Ming-Syan Chen,Fellow,"Exploring Application Level Semantics For Data Compression",IEEE Transactions on Knowledge And Data Engineering,vol 23,No.1,Jan 2011.

[2] S.S. Pradhan, J. Kusuma, and K. Ramchandran, "Distributed Compression in a Dense Microsensor Network," IEEE Signal Processing Magazine, vol. 19, no. 2, pp. 51-60, Mar. 2002.

[3] A. Scaglione and S.D. Servetto, "On the Interdependence of Routing and Data Compression in Multi-Hop Sensor Networks," Proc. Eighth Ann. Int'l Conf. Mobile Computing and Networking, pp. 140-147, 2002.

[4] N. Meratnia and R.A. de By, "A New Perspective on Trajectory Compression Techniques," Proc. ISPRS Commission II and IV, WGII/5, II/6, IV/1 and IV/2 Joint Workshop Spatial, Temporal and Multi-Dimensional Data Modelling and Analysis, Oct. 2003.

[5] C.M. Sadler and M. Martonosi, "Data Compression Algorithms for Energy-Constrained Devices in Delay Tolerant Networks".[6]R. Agrawal and R. Srikant, "Mining Sequential Patterns".

J. Biju, M.E.
Assistant Professor
Department of Computer Science
Theni Kammavar Sangam College of Technology

Theni 625 534
Tamilnadu
India
jbijuinfo@gmail.com

==========
Engineering & Technology in India www.engineeringandtechnologyinindia.com
Vol. 1:2 March 2016
==========

Economic Power Dispatch of Independent Power Producer Using Gray Wolf Optimization

K. Kathiravan and Dr. N. RathinaPrabha

==========

Abstract

Economic Power Dispatch (EPD) is a useful tool for optimal operation and planning of a modern power system. Optimal generation is made to cost effective. Conventional methods have the assumption on fuel cost characteristics of a generating unit which is a continuous and convex function that results fairly satisfied. This proposed work is to design and apply efficient Gray Wolf Optimization (GWO) technique for the solution of optimal generation. Here the non-convex characteristics of the generator along with the ramping limits of the practical generator operation are considered for the computation. By using optimal generation of the conventional method is carried out for 26 bus system with six generating units having ramp rate limits are taken for computation in Matlab environment. The performance of the GWO algorithm is estimated by multi-line contingency and combined bilateral and multilateral wheeling transactions conditions. The results are compared with Autonomous Group of Particle Swarm Optimization (AGPSO) and found GWO method performs better in solving Economic power dispatch problem.

Keywords: Power Flow, Ramp Rate limits, Autonomous Group of Particle Swarm Optimization, Gray Wolf Optimization, Piecewise Linear Ramp Rate

1. Introduction

The power industries have the conventional EPD problem involves a location of different thermal generating units to minimize the operating cost subjected to equality and inequality constraints. The EPD problem is a large scale highly non-linear constrained optimization problem such as linear programming, quadratic programming, non-linear programming, interior

point and Newton-based method. All these methods are made in an assumption that the generation of fuel cost characteristics of a power producer is a smooth and convex function. For example, this situation originates when ramp rate limit and valve-point loading are present in these condition to represent the unit's operating fuel cost characteristics are as convex. So far, the accurate global optimum of the problem could not be reached simply. A novel method is needed to survive with these technique complication and those with high pace search to the optimal and not being fascinated in local minima. In order to optimize the operational cost of power system subjected to the system operating constraints such non- linear problem had explored by Computational Artificial Intelligence (CAI) by many researchers to get optimal solution.

Optimization techniques [1] are meta-heuristics and these are quite simple and inspired by simple concepts typically related with the corporeal phenomena of evolutionary concept and behaviour of animal such meta-heuristics have the flexibility at local optima avoidance. Meta-heuristics are two classes they are single solution based and another is population based. Simulated Annealing (SA) [2] is a search process that starts with the single candidate and improves over the iteration process, Genetic Algorithm (GA) [3] is population based, where the optimization is carried out by set of solutions. Search process start with random initial solution and improved over the iteration process. Artificial Bee Colony (ABC) [4] is the concept of Swarm Intelligence (SI) [5] is coming under the population based meta-heuristics. This Swarm Intelligence (SI) was proposed by Bonabeau, et al [6]. It explains the collective intelligence of group of simple agents. Some of the most popular SI technique are Ant Colony Optimization (ACO) [7], Particle Swarm Optimization (PSO)[8], ABC[4], (AGPSO)[9]. The search process of the meta-heuristics is having the two phases which are exploration and exploitation [10-14] balancing these two phases are challenging task because of stochastic nature. Modified PSO are named as Autonomous Groups of Particles Swarm Optimization (AGPSO) [9]. It is inspired by the individual diversity in swarm flocking (Intersect swarming) which is used for solving high-dimensional problem such as slow convergence rate and trapping in local minima. Every individual in a natural colonies are not similar in ability and intellectual they do their duty as associate member of a colony. In some critical situation each individual's ability is very helpful.

This autonomous group proposed by mathematical model of diverse particles: curvatures,

diverse slopes and interception point are called as functions which are employed to tune the social and cognitive parameter of the particle swarm optimization algorithm. These AGPSO are recently modified in terms of convergence speed and escaping local minima. In this proposed work the Gray wolf optimization (GWO) [15] is used to solve the EPD, non-convex, non-continuous, non-linear cost function. An application was performed on the 26 bus test system with six generating units having the ramping limits [16]. The result obtained through the GWO, AGPSO [9] includes AGPSO1, AGPSO2, AGPSO3, SPSO, MPSO, IPSO, TACPSO which were compared and it confirms the efficacy of likely GWO in terms of upshot excellence, reliability.

2. Problem Formation

Mathematically optimization of fuel cost of each power producers in the system has been formulated based on power flow problem with line flow constraints and the overall generation cost of power system is expressed as following form:

$$\text{Minimize } F(G) = \sum_{j=1}^{ng} (f_j\ (p_j)) \tag{1}$$

Where F(G) is the operating fuel cost of jth power producer and n_g is the number of power producers in the given power system network.

The fuel cost function of a j^{th} power producer is written as:

$$f_j(p_j) = a_j + b_j P_j + c_j\ P_j^2 \quad \$/h \tag{2}$$

Where p_j is active power output of an j^{th} power producer, $f_j(p_j)$ is the fuel cost of j^{th} power producer and a_j, b_j, c_j are the fuel cost co-efficient of the j^{th} power producer.

Power balance constraint is net power generated by the power producers which includes system load demand as well as losses in transmission network.

$$\sum_{j=1}^{ng} p_j - p_l - p_d = 0 \tag{3}$$

Equation (3), is denotes the constraint of power balance equation for EPD, Where p_d is the total load of the system and p_l is transmission losses in the system.

The output level of the power producer which expressed as

$$p_{L=} \sum_{j=1}^{ng} \sum_{k=1}^{ng} B_{jk} p_k p_k + \sum_{j=1}^{ng} p_j B_{j0} B_{00} \quad (4)$$

Equation (5) denotes the Kron's loss formula which approximated the losses as a function of the system output level.

Where $1 \leq j$ and $k \leq ngare$ power producers indexes and B_{jk}, B_{j0}, B_{00} are co-efficient of losses (or) B loss co-efficient. $B_{jk}$is (ng x ng) matrix.

The inequality constraint on real power generation $P_j$of each power producer j is given by:

$$p_{jmin} \leq p_j \leq p_{jmax} \quad (5)$$

Ramp Rate limits is an inequality constraint of the power producer and it can be either increases (or) decreases the power generation.

In 24 hours, horizon all the on-line units have operating ranges which are restricted by their elastic limits or Ramp Rate limits. Whenthepowerproducersoperatewithinthe elastic limits [17-20]. Ifpower producersarepermittedtowidentheirlimits,thelifeoftherotorwillbegetting fatigue. These inequality constraints of Ramp Rate limits are expressed as:

$$p_j - p_{j0} \leq U_{rj} \quad (6)$$

$$p_{j0} - p_j \leq D_{rj} \quad (7)$$

Equation (6 & 7) denote the increase in power generation and decrease in power generation due to Ramp Rate limit U_{rj} and D_{rj} are Ramp up Rate and Ramp down Rate.

Combining (5,6&7) which gives the following equation:

Where is the maximum rating of transmission line connecting p and q.

$$max\ (p_{jmin}, p_{j0} - D_{rj}) \leq p_j \leq min\ (p_{jmax}, p_{j0} + U_{rj}) \quad (8)$$

$$MVAf_{p,q} \leq MVAf_{p,q}^{max} \quad (9)$$

3. Overview of Particle Swarm Optimization

PSO is a robusts to chastic optimization technique based on the movement and cleverness of swarms. Concept of social interaction is applied by PSO for solving a real time problem. InPSOa swarm movesaroundinthesearch spaceandlooksfor theparamountsolution. Eachandeveryparticletracksandcoordinates inthesolution spaces that areassociatedwiththebest fitnessvalueachievedsofarbyaparticularparticle. This value is called personal best (p_{id}).Another best value tracked by the PSO is the best value attained so far by any neighboring particle called global best(p_{gid}).The basic concept of PSO lies in accelerating each particle toward it's (p_{id}) and the (p_{gid}) locations, with a random weighted acceleration at each time step. Eachparticlecorrespondstoacandidatesolutionofthe problem. The particle reaches the optimal solution based on its own experience and the experience of its companions. The velocity of each particle is updated by the following equation:

$$v_{id}^{n+1} = w * v_{id}^{n} + c_1 * rand1 * (p_{id} - x_{id}) + c_2 * rand2 * (p_{gid} - x_{id}) \quad (10)$$

$$x_{id}^{n+1} = x_{id}^{n} + v_{id}^{n+1} \quad (11)$$

Where

v_{id}^{n}	: velocityofagent (i)at iteration
w	:weightingfunction
c_1, c_2	:weightingfactor
rand1, rand2	: uniformlydistributedrandom number (0&1)
x_{id}^{n}	:currentpositionofagent (i)atiteration (n)
p_{id}	:pbestofagent (i),
p_{gid}	:gbestofthe group

ThestepbystepprocedureforPSOalgorithmisgiven asfollows:

- Initializethepositionandvelocityofthe particles.
- Checkstoppingcriteria,if yes stopelsego to step3,

- Checkwhetherallthe particlesarechecked,if no go tostep4 elsego tostep6,
- Computefitnessvalue,
- Update(p_{id})andgo tostep3,
- Computeinertia weight,
- Update(p_{gid}),and Updatevelocity,
- Checkvelocitylimits,
- Updateparticleposition,
- Checkfeasibilitylimitandgotostep2.

3.1 Autonomous group of particle swarm optimization

Particle swarm optimization deals with the fine tuning of the weighing factor c_1 and c_2, by balancing these weighting factor the global minima is found along with the fast convergence speed is also achieved. Here the researchers propose the Autonomous Group Particle Swarm Optimization [9] concept as per modification of the existing PSO technique. In this search space of AGPSO, according to its own strategy is related to the tuning of c_1 and c_2, these autonomous groups contains linear, constant, and exponential of time varying parameters of c_1 and c_2. AGPSO concept is inspired by individual in its group of particle. Individual in a group of particle is not quite same as in their ability and intelligence. Each individual do their duties as a member of workgroup. In some particular situation the ability of individual is very useful to perform their objective. Consider a termite colony that consist of four various termites such as worker, queen, babysitter and solider having various ability to battle with enemies. The diverse ability of an individual in a workgroup is very important for survival from their enemies.

These four termites are considered as four autonomous groups, all termites work together with common objective of their colonys' survival. By using their divergence ability of an individual in an autonomous group with common objective in any population based optimization algorithm hypothetically provides result in additional randomized and direct search concurrently. The mathematical model of Autonomous group PSO are using the various strategies of updating c_1 and c_2, strategies updated by implementing with continuous function with the interval. Those functions may be either ascending or descending linear and polynomial, as well as logarithmic

nature and which are used to update the social factor and cognitive. The modified Autonomous group includes AGPSO1, AGPSO2 and AGPSO3. The dynamic co-efficient of these modified autonomous group are given in Table 1. Here the maximum number of iteration is represented as 'T' and the current iteration is represented as't '.

Table 1. Updating strategies of Autonomous group particle swarm optimization.

Group	Updating strategies of various AGPSO					
	AGPSO1		AGPSO2		AGPSO3	
	c_1	c_2	c_1	c_2	c_1	c_2
G1	$(-2.05/T)^t + 2.55$	$(1/T)^t + 1.25$	$2.5-(2\log(t)/\log(T))$	$(2\log(t)/\log(T)) + 0.5$	$1.95-2t^{1/3}/T^{1/3}$	$2t^{1/3}/T^{1/3} + 0.05$
G2	$(-2.05/T)^t + 2.55$	$(2t^3/T) + 0.5$	$(-2t^3/T^3) + 2.5$	$(2t^3/T^3) + 0.5$	$(-2t^3/T^3) + 2.5$	$(2t^3/T^3) + 0.5$
G3	$(-2t^3/T^3) + 2.5$	$(1/T)^t + 1.25$	$0.5 + 2exp[-(4t/T)^2]$	$2.2-2exp[4t/T)^2]$	$1.95-2t^{1/3}/T^{1/3}$	$(2t^3/T^3) + 0.5$
G4	$(-2t^3/T^3) + 2.5$	$(2t^3/T^3) + 0.5$	$2.5 + 2(t/T)^2 - 2(2t/T)$	$0.5-2(t/T)^2 + 2(2t/T)$	$(-2t^3/T^3) + 2.5$	$2t^{1/3}/T^{1/3} + 0.05$

AGPSO updating strategies contains the logarithmic and exponential functions for c_1 and c_2 which are made effective on the performance of the PSO. These divergent functions are chosen with various curvatures, slopes and intersecting point to examine the effectiveness of these characteristics and to improve the performance of particle swarm optimization. AGPSO could be more efficient and better adaptable than the general PSO in solving a wide range of complex optimization problem.

AGPSO is compared with some modified PSO, the Time varying accelerator are recent modified particle swarm optimization such as SPSO [6], MPSO [21], IPSO [22], TACPSO [23] and their c_1 and c_2 co-efficient are given in Table 2.

Table2. Updating strategies of Modified Particle swarm optimization

Algorithms	Updating strategies of Modified PSO	
	c_1	c_2
SPSO	2	2
MPSO	$(-2.05/T)^t + 2.55$	$(1/T)t + 1.25$
IPSO	$2.5 + 2(t/T)^2 - 2(2t/T)$	$0.5 - 2(t/T)^2 + 2(2t/T)$
TACPSO	$0.5 + 2exp[-(4t/T)^2]$	$2.2-2exp[-(4t/T)^2]$

4. Gray wolf optimization

The Gray wolf optimizer deals with the nature of social behavior of gray wolves towards group hunting with headship hierarchy [15]. To design and execute the optimization, four types of gray wolves are involved they are alpha (α), Beta (β), delta (δ) and omega (ω). The mathematical model of GWO is working for simulating the headship hierarchy besides three main phases of GWO hunting are searching for quarry (chasing, tracking and approaching the quarry),encircling quarry(pursuing and harassing the quarry until it stop moving) and attacking quarry(attack towards the quarry)[15].

The mathematical models of hunting optimization of gray wolves are designed as follows: The first fittest solution as alpha (α), second best solution as Beta (β), third best solution as delta (δ) and the remaining gray wolves are omega (ω) and this is the lowest among the other respectively.

Encircling quarry (pursuing and harassing the quarry until it stops moving) is modelled as follows:

$$\vec{S} = \left|\vec{R} * \overrightarrow{x_\iota}(k) - \vec{x}(k)\right| \quad (12)$$

$$\vec{x}(k+1) = \overrightarrow{x_\iota}(k) - \vec{P} * \vec{S} \quad (13)$$

Where

k : Indicates the present iteration
$\vec{P}$ and $\vec{R}$: Coefficient vector
$\overrightarrow{x_\iota}$: Position vector of the quarry
$\vec{x}$: Position vector of a gray wolf

$\vec{P}$ and $\vec{R}$are calculated as follows:

$$\vec{P} = 2 * \vec{w} * \overrightarrow{c_1} - \overrightarrow{w} \quad (14)$$

$$\vec{R} = 2 * \overrightarrow{c_2} \quad (15)$$

Here $\vec{w}$ decrease linearly from 2 to 0 during the iteration process, $\overrightarrow{c_1}$ and $\overrightarrow{c_2}$ are random vector in [0, 1].

If the gray wolf in some position and it can update its position according to the position of the quarry. From the various positions of the agents the best agent adjusts its current position and reached the quarry by adjusting the co-efficient vectors. Random vectors permit the wolves to reach any position inside the search space around the quarry in any random position by the equation (12) and (13). The hunting is guided by alpha along with beta and delta which hunt together (participating). The alpha, beta and delta have the better knowledge towards location point of the quarry and omegas are updating its position according to the alpha, beta and delta it is mathematically expressed as follows:

$$\overrightarrow{S_\alpha} = \left|\overrightarrow{R_1} * \overrightarrow{x_\alpha} - \vec{x}\right| \quad (16)$$

$$\overrightarrow{S_\beta} = \left|\overrightarrow{R_2} * \overrightarrow{x_\beta} - \vec{x}\right| \quad (17)$$

$$\overrightarrow{S_\delta} = \left|\overrightarrow{R_3} * \overrightarrow{x_\delta} - \vec{x}\right| \quad (18)$$

$$\overrightarrow{x_1} = \overrightarrow{x_\alpha} - \overrightarrow{P_1} * \overrightarrow{S_\alpha} \quad (19)$$

$$\overrightarrow{x_2} = \overrightarrow{x_\beta} - \overrightarrow{P_2} * \overrightarrow{S_\beta} \quad (20)$$

$$\overrightarrow{x_3} = \overrightarrow{x_\delta} - \overrightarrow{P_3} * \overrightarrow{S_\delta} \quad (21)$$

$$\vec{x}(k+1) = \frac{\overrightarrow{x_1} + \overrightarrow{x_2} + \overrightarrow{x_3}}{3} \quad (22)$$

Attacking quarry or exploitation by the gray wolves finishes the quarry when it stops moving. In mathematically this can be expressed as by decreasing the value of the $\vec{w}$ likewise the $\vec{P}$ also decrease from 2 to 0 in the overall iteration. When $\vec{P}$ are in [-1, 1], the next location point of the search agent can be in any location between its current location point and the location point of the quarry if $\left|\vec{P}\right| < 1$ the strength of the wolves assault in the direction of the quarry. Therefore Gray wolf optimizer algorithm allows its wolves to update the location point based on the alpha, beta and delta wolves and hunting towards the quarry which is the local best solution. The vector $\vec{P}$ is utilized with an unsystematic value higher than 1 or lesser than -1 to fondness the wolves to diverge from the quarry and it emphasizes the look for quarry and let the gray wolf optimizer to search globally. Another component $\vec{R}$ to exploration it contains unsystematic values[0, 2] and it provides the unsystematic weight of the quarry to $\vec{R} > 1$ or $\vec{R} < 1$ the effect of quarry in defining the distance and it help to GWO as more unsystematic behaviour during the optimization, which favour the searching and the avoidance of local optimum solution. $\vec{R}$is not

linearly reduce in contrast of $\vec{P}$ and this component is very useful in final iteration. Finally the GWO algorithm stops by fulfilment of the end criterion.

5. Simulation Result and Discussions

The operation of the generating unit is narrow with their power limits (real and reactive). But in real situation load commitments beyond their power limits for a given time duration contingencies, multiple contingencies combined bilateral and multilateral wheeling transactions. This type of functioning will cause rotor fatigue. Even though reliability of power system operation must need to take care and this operation is foreseeable. Therefore, generating units are realistically compensated by the system operators. The change in state of their operation is also narrow by their RR limits. If any violation regarding the elastic RR limits for maintaining the system protection. The RR limits and fuel cost are taken from [16].The power producer has operating power limits and operating power along with the RR limit to get new operating power limits shown below in Table 3.

Table 3. Power generation limits after adding Ramp Rate limits

Gen no.	P_{jmin}	P_{jmax}	P_{i0}	Drj	Urj	$P_j'_{min}$	$P_j'_{max}$	a_j	b_j	C_j
G1	100	500	440	80	120	321	500	240	7	0.0070
G2	50	200	170	50	90	80	200	200	10	0.0095
G3	80	300	200	65	100	101	266	220	8.5	0.0090
G4	50	150	150	50	90	60	150	200	11	0.0090
G5	50	220	190	50	90	100	220	220	10.5	0.0085
G6	50	120	111	50	90	50	120	190	12	0.0075

5.1 Sixgenerating units of 26bus test system

The optimal generating cost of the power producers were obtained using AGPSO1, AGPSO2, AGPSO3, MPSO, SPSO, IPSO,TACPSO and GWO algorithm, when subjected with base load condition, multiple contingency and combined bilateral and multilateral wheeling transactions.

5.1.1 Case 1: Base Load Condition

The power flow is carried out for the test system with the 100 base MVA, and the load demand 1263. B loss co-efficient (Boo) of test bus system is taken from [16] is shown below in Table 4.

Table 4. B loss co-efficient for 26 bus test system (base load)

B	0.0017 0.0012 0.0007 -0.0001 -0.0005 -0.0002 0.0012 0.0014 0.0009 0.0001 -0.0006 -0.0001 0.0007 0.0009 0.0031 0.0000 -0.0010 -0.0006 -0.0001 0.0001 0.0000 0.0024 -0.0006 -0.0008 -0.0005 -0.0006 -0.0010 -0.0006 0.0129 -0.0002 -0.0002 -0.0001 -0.0006 -0.0008 -0.0002 0.0150
B0	1.0e-003 * (-0.3908 -0.1297 0.7047 0.0591 0.2161 -0.6635)
B00	0.0056

With this base load the optimal generation cost is obtained through the AGPSO1, AGPSO2, AGPSO3, MPSO, SPSO, IPSO,TACPSO and GWO algorithm and the obtained minimal fuel cost values are compared which are shown below in Table 5.

Table 5. Comparison among different method (base load)

	Conventional method	Optimization method							
Gen no.	**NR method ($/h)**	**AGPSO1 ($/h)**	**AGPSO2 ($/h)**	**AGPSO3 ($/h)**	**MPSO ($/h)**	**SPSO ($/h)**	**IPSO ($/h)**	**TACPSO ($/h)**	**GWO ($/h)**
Gen1	447.6919	500	424.872	490.0655	424.872	490.0895	500	500	437.9554
Gen2	173.1938	200	158.687	126.2701	158.687	182.9178	128.9369	200	180.8478
Gen3	263.4859	249.6076	255.2737	238.8003	255.2737	213.0125	266	248.3405	262.8706
Gen4	138.8142	93.398	146.1874	92.4557	146.1874	103.2731	97.1421	60	127.6967
Gen5	165.5884	100	196.0959	195.4141	196.0959	219.9512	218.8271	134.6651	174.1308
Gen6	87.0260	120	81.8896	120	81.8896	53.7615	52.0995	120	79.4987
Min F(G)	15447.72	15366.286	15290.124	15338.096	15288.263	15343.276	15344.918	15365.412	**15278.120**
Pd	1263								
B loss	0.0056								

From Table 5, it is obvious that, GWO gives the best optimal cost of generation for the test system under Base load condition. The converged characteristic of the AGPSO1, AGPSO2, AGPSO3, MPSO, SPSO, IPSO, TACPSO and GWO algorithm for the base load condition are shown in the Fig 1.

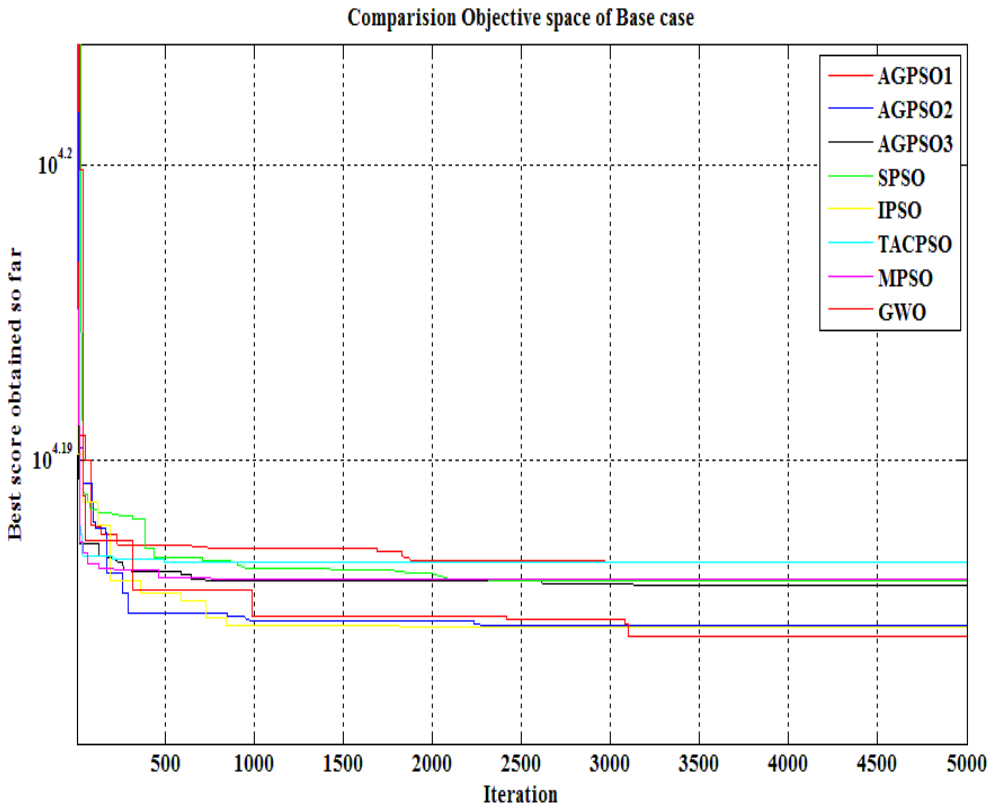

Fig 1. Converged characteristic of AGPSO and GWO in base load condition

5.1.2 Case 2: Optimal Production Cost with multiple Line Contingency

In this case, the optimal generation cost of the test system obtained through the AGPSO1, AGPSO2, AGPSO3, MPSO, SPSO, IPSO,TACPSO and GWO, when subjected to multiple line contingency is illustrated by making the transmission line between the buses are shown in the Table 6.

Table 6. Multiple contingency (transmission line outage)

Transmission line(outage)	From bus	To bus
Line1	2	8
Line2	4	8
Line3	7	8

The B loss co-efficient (Boo) were calculated from [24] for multiline contingency conditions are given in the Table 7.

Table 7. B loss co-efficient for multiple contingency

B	0.0021 0.0014 0.0009 -0.0012 -0.0004 0.0000 0.0014 0.0015 0.0012 -0.0008 -0.0004 0.0001 0.0009 0.0012 0.0033 -0.0003 -0.0010 -0.0005 -0.0012 -0.0008 -0.0003 0.0068 -0.0016 -0.0017 -0.0004 -0.0004 -0.0010 -0.0016 0.0143 0.0000 0.0000 0.0001 -0.0005 -0.0017 0.0000 0.0155
B0	-0.0007 -0.0001 0.0006 0.0015 -0.0002 -0.0009
B00	0.0054

With this multiline contingency condition the optimal generation cost is obtained through the AGPSO1, AGPSO2, AGPSO3, MPSO, SPSO, IPSO,TACPSO and GWO algorithm.

The obtained minimal fuel cost values are compared which are shown below in the Table 8.
From Table 8, it is obvious that, GWO gives the best optimal cost of generation for multiple line contingency condition.

Table 8. Comparison among different method (Multiple contingency)

Gen no.	Conventional method	Optimization method							
	NR method ($/h)	**AGPSO1 ($/h)**	**AGPSO2 ($/h)**	**AGPSO3 ($/h)**	**MPSO ($/h)**	**SPSO ($/h)**	**IPSO ($/h)**	**TACPSO ($/h)**	**GWO ($/h)**
Gen1	446.1992	500	425.7235	499.9416	425.7235	474.9777	470.4662	483.7859	455.7907
Gen2	173.1159	169.6639	194.069	171.1887	194.069	130.012	200	163.787	172.5812
Gen3	262.3577	248.2813	254.2706	254.5442	254.2706	216.7298	262.1636	235.0527	265.6533
Gen4	143.8471	103.1171	111.946	85.841	111.946	132.8012	106.2751	110.3797	122.4546
Gen5	164.5505	191.9431	156.9963	162.559	156.9963	198.4116	141.8093	220	162.0017
Gen6	86.9847	50	120	88.9332	120	110.073	82.2912	50	84.5217
Min F(G)	15465.95	15314.16	15298.25	15311.81	15283.47	15329.26	15298.42	15322.53	**15277.69**
Pd	1263								
B loss	0.0054								

The converged characteristics of the AGPSO1, AGPSO2, AGPSO3, MPSO, SPSO, IPSO,TACPSO and GWO algorithm for the multiple line contingency condition of the test bus system shown in Fig 2.

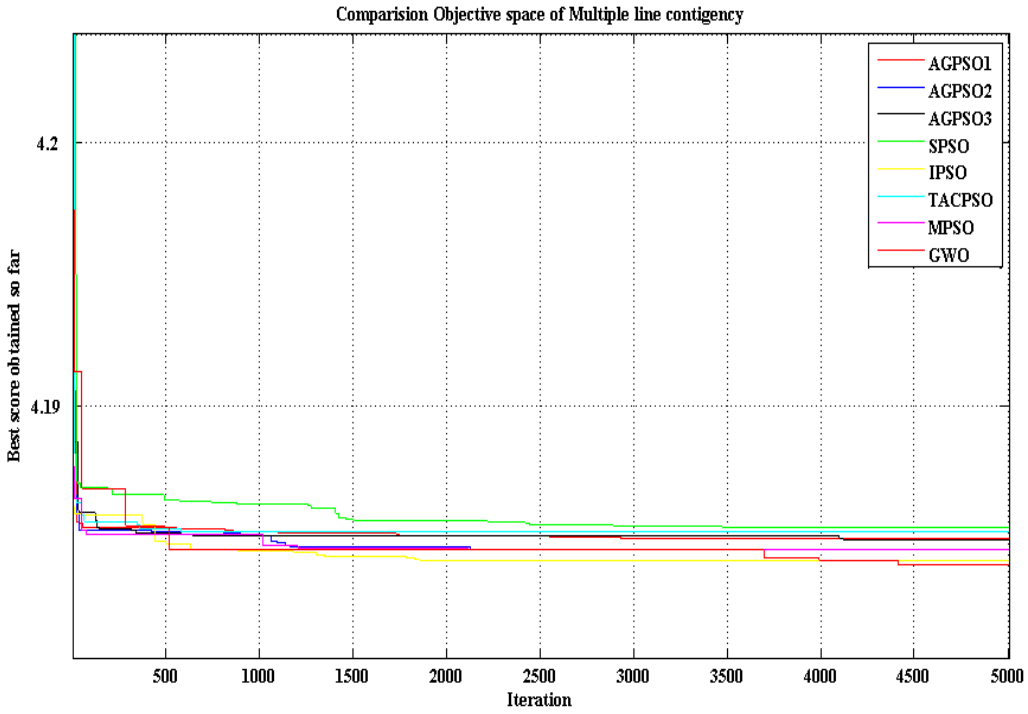

Fig 2. Converged characteristic of PSO and GWO in multiple contingency conditions

5.1.3 Case 3: Optimal Production Cost with Wheeling Transactions (Combined Bilateral and Multilateral)

In this case, the optimal generation cost of the test system obtained through the AGPSO1, AGPSO2, AGPSO3, MPSO, SPSO, IPSO, TACPSO and GWO, when subjected tocombined Bilateral and multilateral wheeling transaction is illustrated by making the transmission line between the buses are shown in Table 9 and the B loss co-efficient (Boo) were calculated from [24] for the test bus system under combined bilateral and multilateral transaction condition are shown below in the Table 10.

With this combined bilateral and multilateral wheeling transaction condition the optimal generation cost is obtained through the AGPSO1, AGPSO2, AGPSO3, MPSO, SPSO, IPSO, TACPSO and GWO algorithm

Table 9. Combined wheeling transaction (Bilateral and Multilateral)

Transmission Transaction	Bus no			Transaction in (MW)
	From bus	**Real power (MW)**	**To bus**	
Bilateral	22	10	25	10
Multilateral	12	30	11	15
			16	15

Table 10. B loss co-efficient for combined wheeling transaction (Bilateral and Multilateral)

B	0.0017 0.0012 0.0007 -0.0000 -0.0005 -0.0003 0.0012 0.0014 0.0010 0.0001 -0.0006 -0.0002 0.0007 0.0010 0.0031 0.0001 -0.0010 -0.0007 -0.0000 0.0001 0.0001 0.0025 -0.0005 -0.0008 -0.0005 -0.0006 -0.0010 -0.0005 0.0129 -0.0003 -0.0003 -0.0002 -0.0007 -0.0008 -0.0003 0.0150
B0	1.0e-003 *(-0.3681 -0.1101 0.7157 0.1357 0.2197 -0.8027)
B00	0.0056

The obtained minimal fuel cost values are compared which are shown below in Table 11.

Table 11. Comparison among different method (Combined wheeling transaction)

Gen no.	Conventional method	Optimization method							
	NR method ($/h)	**AGPSO1 ($/h)**	**AGPSO2 ($/h)**	**AGPSO3 ($/h)**	**MPSO ($/h)**	**SPSO ($/h)**	**IPSO ($/h)**	**TACPSO ($/h)**	**GWO ($/h)**
Gen1	447.5274	444.4629	426.1049	497.9179	426.1049	467.1361	442.4508	463.0382	444.5812
Gen2	173.1008	137.9018	200	200	200	121.8754	165.6139	163.6915	169.0726
Gen3	263.5652	266	251.7548	237.6882	251.7548	267.3993	252.2818	217.7978	263.8072
Gen4	137.8124	131.834	133.5718	92.3326	133.5718	126.6185	135.0405	137.7616	127.0212
Gen5	165.5949	176.7804	131.5739	162.1056	131.5739	207.683	162.1821	199.3394	171.2
Gen6	88.5448	106.0263	120	72.9611	120	72.2932	105.4363	81.3769	87.3273
Min F(G)	15452.15	15290.98	15311.91	15319.87	15295.86	15313.29	15282.92	15305.09	**15276.68**
Pd	1263								
B loss	0.0056								

From Table 11, it is obvious that, GWO gives the best optimal cost of generation for the test system under combined bilateral and multilateral wheeling transaction condition.

The converged characteristic of the AGPSO1, AGPSO2, AGPSO3, MPSO, SPSO, IPSO, TCPSO and GWO algorithms for combined bilateral and multilateral wheeling transaction condition of the test bus system is shown in Fig 3.

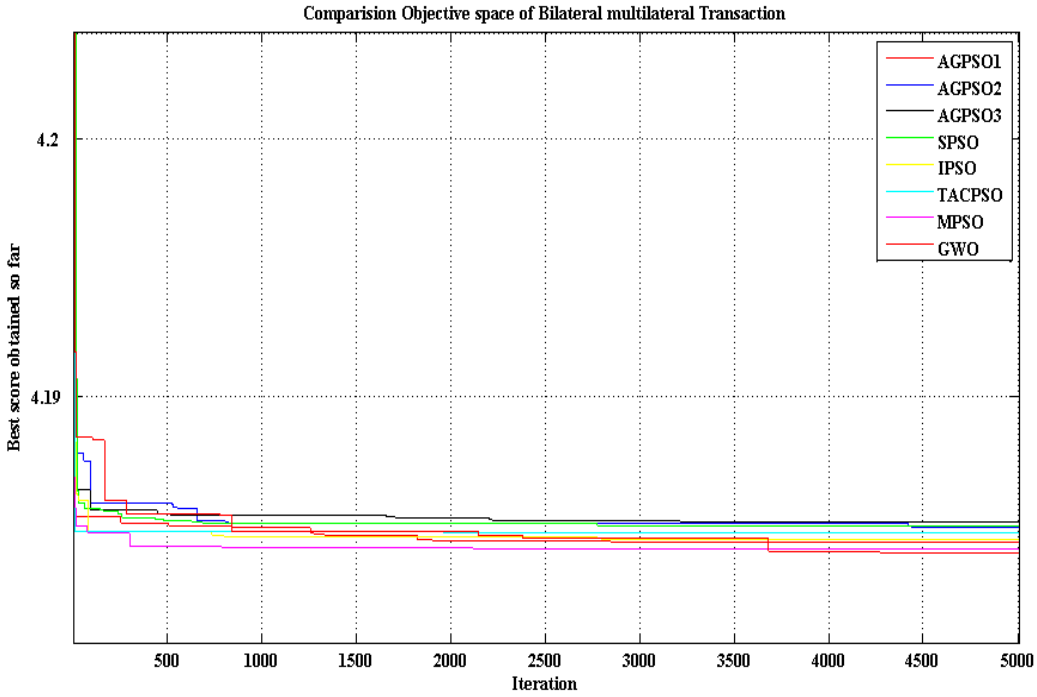

Fig 3. Converged characteristic of PSO and GWO in (Combined wheeling transaction)

The optimal generating cost of the power producers were obtained using Autonomous Group PSO and GWO algorithms along with transmission line constraints. The power flows carried out through the conventional method (Newton-Raphson) and bus loss co-efficient (Boo) were calculated. The result obtained here for base case was near around results from [16].The usefulness of the proposed technique has been performed on the 26bus test system with 6 generating units having ramp rate limits under different cases such as combined bilateral and multilateral Transaction and multiple transmission line contingency condition. The simulation studies were carried out on Intel Pentium Dual Core, 2 GHz system in MATLAB environment.

6. Conclusion

This proposed work explained the social behaviour, headship hierarchy and hunting optimization mechanism of the gray wolves, for solving the EPD problem. This GWO algorithm

has the better optimum performance than the Autonomous group particle swarm optimization which includes AGPSO1, AGPSO2, AGPSO3, MPSO, IPSO, TACPSO, SPSO and other heuristic algorithms. The proposed algorithm demonstrated for the 26 bus test system with Ramp rate limit considering multiple contingency as well as combined bilateral and multilateral wheeling transactions. The compared results give the feasible economic dispatch to the producer to meet the load demand when subjected at any cause of risk condition to the power system. More over this GWO algorithm has betterperformance in both constraints as well as unconstraint problem.

==========

References

[1] R.C. Bansal, Optimization methods for electric power system: An overview, International Journal of Emerging Electric Power Systems, Vol.2 No.1, article (2005) 1021.

[2] S.Kirkpatrick, DG.Jr, MP.Vecchi, Optimization by simulated annealing, Science. Vol.220 (1983) 671-680.

[3] JH.Holland, Genetic Algorithm, Science Am 267 (1992) 66-72.

[4] B.Basturk, D.Karaboga, An Artificial Bee Colony (ABC) algorithm for numeric function optimization, IEEE swarm intelligence symposium. (2006) 12-14.

[5] G.Beni, J.Wang, Swarm intelligence in cellular Robotic systems, Robots and biological system: towards a new bionics? ed. Springer. (1993) 703-712.

[6] E.Bonabeau, M.Dorigo, G.Theraulaz, Swarm intelligence: from natural to artificial system: OUP USA (1999).

[7] M.Dorigo, M. Birattari, T. Stutzle, Ant colony optimization, IEEE computation Intelligence Magazine.1 (2006) 28-39.

[8] R.C.Eberhart, J.Kennedy, Particle swarm optimization, IEEE International conference on Neural Network, Perth, Australia. (1995) 1942-1948.

[9] S.Mirjalili, A.Lewis, A.SafaSadiq, Autonomous Particle Groups for Particle Swarm optimization,Arab.j.SciEng,vol.39(2014) Issue 6 4683-4697.

[10] O.Olorunda, AP. Engelbrecht, Measuring exploration/exploitation in particle swarms using

swarm diversity, IEEE Congress Evolutionary computation, (IEEE World congress on computational Intelligence), CEC (2008) 1128-1134.

[11] E.Alba, B.Dorronsoro, The exploration /exploitation trade off in dynamic cellular genetic algorithms, IEEE Transaction on Evolutionary computation, Vol.9 (2005) 126-142.

[12] L.Lin, M.Gen, Auto-tuning strategy for evolutionary algorithms: balancing between exploration and exploitation, Soft Computing, Vol.13 (2009) 157-168.

[13] S.Mirjalili, S.Z. Mohammed Hashim, a new hybrid PSOGSA algorithm for function optimization, International conference on Computer and information application (ICCIA),(2010) 374-377.

[14] S.Mirjalili, S.Z. Mohammed Hashim, H.MoradianSardroudi, Training feed forward neural networks using hybrid particle swarm optimization and gravitational search algorithm, Applied Math Computation, Vol.218 (2012) 11125-11137.

[15] S.Mirjalili, S. Mohammad Mirjalili, Andrew Lewis, Grey Wolf Optimizer, Advance in Engineering Software,Vol. 69 (2014) 46-61.

[16] Jun sun, Vasile Palade, Xiao-Jun Wu, Wei Fang, Zhenyu Wang, Solving the Power Economic Dispatch Problem with Generator Constraints by Ramndom Drift Particle Swarm Optimization, IEEE Transaction on Industrial Vol. 10 No.1 February (2014) 222-232.

[17] C.Wang, S.Mohammed, Optimal generation scheduling with ramping costs, IEEE Transaction on power system, Vol.10, No.1 February(1995) 60-67.

[18] G.B.Shreshtha, K.Song, L.Goel, Strategic self-dispatch considering ramping costs in deregulated power market, IEEE Transaction on power system, Vol.19, No.3 August (2004) 1575-1581.

[19] M. Tanaka, Real time pricing with ramping cost: A new approach to managing a steep change in electricity demand, International Journal of Energy Policy, Vol.34, No.18 December (2006) 3634-3643.

[20] T.Li, M.Shahidehpour, Dyanamic ramping in unit commitment, IEEE Transaction on Power system, Vol .22, No.3 August (2007) 1379-1381.

[21] Z.Cui, J Zeng, Y.Yin, An improved PSO with time-varying accelerator coefficients, Eighth International conference on intelligent systems design and applications, Kaohsiung (2008) 638-643.

[22] T.Ziyu, Z.Dingxue, AA modified particle swarm optimization with an adaptive acceleration coefficient, Asia-pacific conference on Information Processing, Shenzhen (2009) 330-332.

[23] G.Q.Bao, K.F.Mao, Particle swarm optimization algorithm with asymmetric time varying acceleration coefficient, IEEE International Conference on Robotics and Biomimetics, Guilin (2009) 2134-2319.

[24] H.Saadat, Power System Analysis, McGraw-Hill Publication, Chapter 7, (1999) 300-302.

K.Kathiravan (Corresponding Author)
Department of Electrical and Electronics Engineering
Theni KammavarSangam College of Technology
Theni-625 534
Tamilnadu
India
electrickathir786@gmail.com

Dr. N. RathinaPrabha
Associate Professor
Department of Electrical and Electronics Engineering
MepcoSchlenk Engineering College
Sivakasi – 626005
Tamilnadu
India
nrp_me@yahoo.co.in
nrpeee@mepcoeng.ac.in

==========
Engineering & Technology in India www.engineeringandtechnologyinindia.com
Vol. 1:2 March 2016
==========

An Inventory Model with Weibull Deterioration Rate Under the Delay in Payment in Demand Declining Market with Salvage Value

Ms. K. Muthulakshmi, M.Sc., B.Ed., M.Phil.

==========

ABSTRACT

In this paper, we purposed an Economic Order Quantity (EOQ) based model for deteriorating items with weibull deterioration in a declining market when the supplier offers a permissible delay in payments to the retailer to settle the account against the purchases. The algorithm is exhibited for an retailer to determine the optimal order quantity which minimizes the total inventory cost per time unit. A numerical example is given to demonstrate the optimal decision for the retailer. The sensitivity analysis is carried out to analysis the changes in the changes in optimal solution with respect to other different parameter.

Keywords: Weibull Deterioration, lot size, trade credit, declining demand, salvage value.

1. INTRODUCTION

Inventory models play an important role in operations research and management science. It is an integral part of logistic systems common to all sectors of economy. Because of the importance of this branch of decision making in a number of practical situations in Government, military organizations, industries, hospitals etc.; significant development of the subject in new directions resulted. The main factors affecting the inventory are demand, lifetime of items stored, production rate, lead time, damage rate due to external disaster, availability of space in store etc.

If all the parameters are known before hand, then the inventory model is called deterministic inventory model. If some or all of these parameters are not known with certainty, then it is justifiable to consider them as random variables with some probability distributions and the resulting inventory model is then called stochastic inventory model. There can be single or

multi-commodity inventory systems. Inventory systems may again be classified as continuous review or periodic review. In continuous review, the system is monitored continuously over time. In periodic review systems, the system is monitored at discrete, equally spaced instants of time.

Inventories are materials stored, waiting for processing, or experiencing processing. They are ubiquitous throughout all sectors of the economy. Observation of almost any company balance sheet, for example, reveals that a significant portion of its assets comprises inventories of raw materials, components and subassemblies within the production process, and finished goods. Most managers don't like inventories because they are like money placed in a drawer, assets tied up in investments that are not producing any return and, in fact, incurring a borrowing cost. They also incur costs for the care of the stored material and are subject to spoilage and obsolescence. In the last two decades their have been a spate of programs developed by industry, all aimed at reducing inventory levels and increasing efficiency on the shop floor.

Manoj Kumar Mehar, Gobinda Chandra Panda, Sudhir Kumar Sahu (2012)[30] consider the demand of a product is assumed to be decreasing with time. The decrease in demand is observed for fashionable garments, seasonal products etc. Shortages are not allowed and replenishment rate is infinite. Here the deterioration is considered as weibull function of time. It is assumed that the retailer generates revenue on unit selling price which is necessary higher then the unit purchase cost. The total cost of an inventory system per time is minimized. The model is supported by a numerical example. The sensitivity analysis is carried out to observe the changes in the optimal solution.

2. NOTATIONS

Following are the notations and assumptions for the development of proposed model.

1. R(t)=a(1-bt) is the annual demand rate which is decreasing function of time where a>0 is fixed demand and b(0<b<1) denote the rate of demand.
2. C is the unit purchase cost
3. P is the unit selling price with (P>C)
4. h is the inventory holding cost per unit per year excluding interest charges.
5. A is the order cost per order.

6. M is the permissible credit period offered by the suppler to the retailer for settling the account.
7. I_c is then interest rate charged per monetary unit in stock per annum by the supplier.
8. I_e is the interest rate earned per monetary unit per year($I_c > I_e$)
9. Q is the order quantity
10. Θ(t) is deteriorating rate which is a weibull function of time as
    Θ (t) =$\alpha\beta t^{\beta-1}$ ($\alpha>0$, $\beta>0$ & $t>0$)
11. $I(t)$ is inventory level at any instant of time t,($0 \le t \le T$)
12. T is the replenishment cycle time
13. S is the salvage value per unit time
14. K(T) is the total inventory cost per time unit

The total cost of inventory system consists of (a) order cost (b) cost due to deterioration, (c) Inventory holding cost (d) interest charged on unsold item after the permissible trade credit when M<T, and (e) interest earned from sales revenue during the allowable permissible delay period.

3. ASSUMPTIONS

1. The inventory system under consideration deals with the single item.
2. The planning horizon is infinite.
3. The demand of the product is declining function of the time.
4. Shortages are not allowed and lead-time is zero.
5. The deteriorated units can neither be repaired nor replaced during the cycle time.
6. The salvage value ¥ ($0 \le ¥ \le 1$) is associated to deteriorated units during the cycle time.
7. The retailer can deposit generated sales revenue in an interest bearing account during the permissible credit period. At the end of this period the retailer settles the account for all the units sold keeping the difference for day-to-day expenditure, and paying the interest charges on the unsold items in the stock.

4. MATHEMATICAL MODEL

The inventory level I(t) depletes to meet the demand and deterioration. The rate of change of inventory level is governed by the following differential equation.

$$\frac{dI(t)}{dt} + \theta I(t) = -R(t) \quad ; \quad 0 \le t \le T \tag{1}$$

Which is equivalent to

$$\frac{dI(t)}{dt} + \alpha t^{\beta-1} I(t) = -a(1-bt) \quad ; \quad 0 \le t \le T \tag{2}$$

With the initial condition I(0) =Q and the boundary condition I(T)=0.

Consequently, the solution of (2) is given by

Put $I(t) = y$; $t = x$ in eqn (2), we get,

$$\frac{dy}{dx} + \alpha x^{\beta-1} y = -a(1-bx)$$

Let $P = \alpha x^{\beta-1}$; $Q = -a(1-bx)$

$$\int P dx = \int \alpha x^{\beta-1} dx$$

$$= \alpha \left(\frac{x}{\beta} \right)$$

$$= \alpha x$$

$$e^{\int P dx} = e^{\alpha x}$$

$$y e^{\int P dx} = \int Q e^{\int P dx} dx + c$$

$$y e^{\alpha x} = \int_T^t -a(1-bx) e^{\alpha x} \, dx + c$$

$$I(t) = a e^{-\alpha t} \left\{ \begin{array}{l} \left[T - t\right] + \frac{\alpha}{\beta+1}\left[T^{\beta+1} - t^{\beta+1}\right] \\ -\frac{b}{2}\left[T^2 - t^2\right] - \frac{b\alpha}{\beta+2}\left[T^{\beta+2} - t^{\beta+2}\right] \end{array} \right\} \tag{3}$$

The order quantity is

$$I(0) = a e^{-\alpha(0)} \left\{ \begin{array}{l} \left[T - 0\right] + \frac{\alpha}{\beta+1}\left[T^{\beta+1} - 0^{\beta+1}\right] \\ -\frac{b}{2}\left[T^2 - 0^2\right] - \frac{b\alpha}{\beta+2}\left[T^{\beta+2} - 0^{\beta+2}\right] \end{array} \right\}$$

$$I(0) = a e^{0} \left\{ \begin{array}{l} [T] + \frac{\sim}{+1}[T^{+1}] \\ -\frac{b}{2}[T^{2}] - \frac{b\sim}{+2}[T^{+2}] \end{array} \right\}$$

$$Q = I(0) = a\left\{ T + \frac{\sim T^{+1}}{+1} - \frac{bT^{2}}{2} - \frac{b\sim T^{+2}}{+2} \right\} \tag{4}$$

The total cost of inventory system per time unit includes the followings:

(a) Ordering cost

$$OC = \frac{A}{T} \tag{5}$$

(b) Deterioration cost per unit time:

$$DC = \frac{C}{T}\left[Q - \int_{0}^{T} a(1-bt)dt \right]$$

$$= \frac{C}{T}\left[a\left\{ T + \frac{\sim T^{+1}}{+1} - \frac{bT^{2}}{2} - \frac{b\sim T^{+2}}{+2} \right\} - \int_{0}^{T} a(1-bt)dt \right]$$

$$DC = \frac{a\sim C}{T}\left[\frac{T^{+1}}{+1} - \frac{bT^{+2}}{+2} \right] \tag{6}$$

Inventory holding cost per unit time:

$$HC = \frac{h}{T}\int_{0}^{T} I(t)dt$$

$$= \frac{h}{T}\int_{0}^{T} a e^{-\sim t} \left\{ \begin{array}{l} [T-t] + \frac{\sim}{+1}[T^{+1} - t^{+1}] \\ -\frac{b}{2}[T^{2} - t^{2}] - \frac{b\sim}{+2}[T^{+2} - t^{+2}] \end{array} \right\} dt$$

$$= \frac{ah}{T}\int_{0}^{T} (1 - \sim t + ...) \left\{ \begin{array}{l} [T-t] + \frac{\sim}{+1}[T^{+1} - t^{+1}] \\ -\frac{b}{2}[T^{2} - t^{2}] - \frac{b\sim}{+2}[T^{+2} - t^{+2}] \end{array} \right\} dt$$

$$HC = \frac{ah}{T}\left\{\begin{array}{l} \dfrac{b\sim {}^{2}T^{2\ +3}}{(\ \ +1)(2\ \ +3)} - \dfrac{\sim {}^{2}T^{2\ +2}}{2(\ \ +1)^{2}} \\ -\dfrac{b\sim\ T^{\ +3}}{(\ \ +1)(\ \ +3)} \\ +\dfrac{\sim\ T^{\ +2}}{(\ \ +1)(\ \ +2)} - \dfrac{bT^{3}}{3} + \dfrac{T^{2}}{2} \end{array}\right\} \qquad (7)$$

Inventory Model with Weibull Deterioration Rate

Inventory model

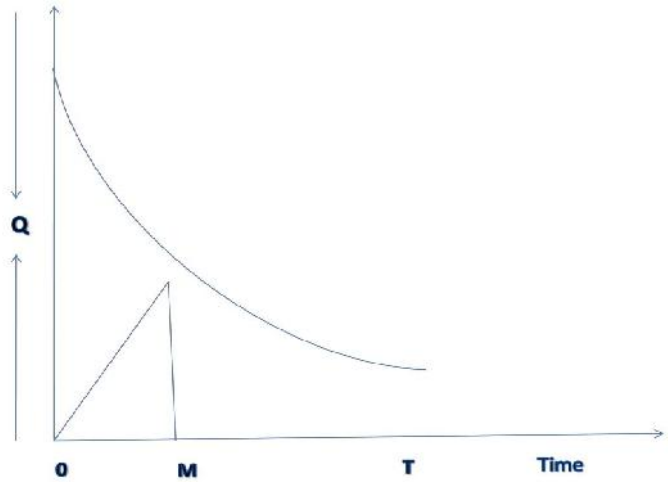

Fig -1 (M < T)

CASE 1: $M < T$

Under the assumption the retailer sells R(M) M units by the end of the permissible tread credit M and has CR(M) M to pay the supplier. For the unsold items in the stock, the supplier charges an interest rate from time M onwards. Hence the interest charged, IC_1 per time unit is

$$IC_1 = \frac{CI_c}{T}\int_{M}^{T} I(t)dt$$

$$IC_1 = \frac{CI_c}{T}\int_{M}^{T} ae^{-\sim t}\left\{\begin{array}{l} [T-t] + \dfrac{\sim}{+1}\left[T^{\ +1} - t^{\ +1}\right] \\ -\dfrac{b}{2}\left[T^{2} - t^{2}\right] - \dfrac{b\sim}{+2}\left[T^{\ +2} - t^{\ +2}\right] \end{array}\right\} dt$$

$$IC_1 = \frac{aCI_c}{T}\int_M^T (1 - \sim t \quad + ...)\left\{\begin{array}{l}[T-t] + \frac{\sim}{+1}\left[T^{\ +1} - t^{\ +1}\right] \\ -\frac{b}{2}\left[T^2 - t^2\right] - \frac{b\sim}{+2}\left[T^{\ +2} - t^{\ +2}\right]\end{array}\right\} dt$$

$$= \frac{aCI_c}{T}\left\{\begin{array}{l}\int_M^T T dt - \int_M^T t dt + \frac{\sim}{+1}\int_M^T T^{\ +1} dt - \frac{\sim}{+1}\int_M^T t^{\ +1} dt - \frac{b}{2}\int_M^T T^2 dt \\ + \frac{b}{2}\int_M^T t^2 dt - \frac{b\sim}{+2}\int_M^T T^{\ +2} dt + \frac{b\sim}{+2}\int_M^T t^{\ +2} dt - \sim \int_M^T Tt \ \ dt \\ + \sim \int_M^T t^{\ +1} dt - \frac{\sim^2}{+1}\int_M^T T^{\ +1} t \ \ dt + \frac{\sim^2}{+1}\int_M^T t^{2\ +1} dt + \frac{b\sim}{2}\int_M^T T^2 t \ \ dt \\ - \frac{b\sim}{2}\int_M^T t^{\ +2} dt + \frac{b\sim^2}{+2}\int_M^T T^{\ +2} t \ \ dt - \frac{b\sim^2}{+2}\int_M^T t^{2\ +2} dt\end{array}\right\}$$

$$IC_1 = \frac{aCI_c}{T}\left\{\begin{array}{l}\frac{T^2}{2} - \frac{bT^3}{3} + \frac{\sim T^{\ +2}}{(\ +1)(\ +2)} - \frac{\sim^2 T^{2\ +2}}{2(\ +1)^2} \\ - \frac{b\ \sim T^{\ +3}}{2(\ +1)(\ +3)} + \frac{b\sim^2 T^{2\ +3}}{(\ +1)(2\ +3)} \\ - \left(\frac{\sim T^{\ +1}}{+1} - \frac{b\sim T^{\ +2}}{+2} - \frac{bT^2}{2} + T\right)\left(M - \frac{\sim M^{\ +1}}{+1}\right) \\ - \frac{\sim\ M^{\ +2}}{(\ +1)(\ +2)} + \frac{M^2}{2} - \frac{bM^3}{6} + \frac{b\sim\ M^{\ +3}}{2(\ +2)(\ +3)} \\ - \frac{\sim^2 M^{2\ +2}}{(\ +1)(2\ +2)} + \frac{b\sim^2 M^{2\ +3}}{(\ +2)(2\ +3)}\end{array}\right\} \qquad (8)$$

During [0,M] the retailer sells the product and deposits the revenue into an interest earning account at the rate I_e per monetary unit per year. Therefore, the interest earned, IE_1 per unit time is

$$IE_1 = \frac{PI_e}{T}\int_0^M R(t)tdt$$

$$= \frac{PI_e}{T}\int_0^M a(1-bt)tdt$$

$$= \frac{PI_e}{T}\int_0^M (at - abt^2)dt$$

$$IE_1 = \frac{aPI_e}{T}\left(\frac{M^2}{2} - \frac{bM^3}{3}\right) \tag{9}$$

Salvage value

$$S = ¥(DC)$$

$$= ¥\left\{\frac{a\sim C}{T}\left[\frac{T^{+1}}{+1} - \frac{bT^{+2}}{+2}\right]\right\}$$

$$S = \frac{¥a\sim C}{T}\left[\frac{T^{+1}}{+1} - \frac{bT^{+2}}{+2}\right] \tag{10}$$

Hence, the total cost of an inventory system for M< T per time unit is

$$K_1(T) = OC + DC + IE_1 + HC + IC_1 - S$$

$$K_1(T) = \left(\begin{array}{l} \frac{aCI_c}{T}\left\{\begin{array}{l} \frac{T^2}{2} - \frac{bT^3}{3} + \frac{\sim T^{+2}}{(+1)(+2)} - \frac{\sim^2 T^{2+2}}{2(+1)^2} \\ -\frac{b\sim T^{+3}}{2(+1)(+3)} + \frac{b\sim^2 T^{2+3}}{(+1)(2+3)} \\ -\left(\frac{\sim T^{+1}}{+1} - \frac{b\sim T^{+2}}{+2} - \frac{bT^2}{2} + T\right)\left(M - \frac{\sim M^{+1}}{+1}\right) \\ -\frac{\sim M^{+2}}{(+1)(+2)} + \frac{M^2}{2} - \frac{bM^3}{6} + \frac{b\sim M^{+3}}{2(+2)(+3)} \\ -\frac{\sim^2 M^{2+2}}{(+1)(2+2)} + \frac{b\sim^2 M^{2+3}}{(+2)(2+3)} \end{array}\right\} + \frac{A}{T} + \frac{a\sim C}{T}\left[\frac{T^{+1}}{+1} - \frac{bT^{+2}}{+2}\right] \\ + \frac{aPI_e}{T}\left(\frac{M^2}{2} - \frac{bM^3}{3}\right) - \frac{¥a\sim C}{T}\left[\frac{T^{+1}}{+1} - \frac{bT^{+2}}{+2}\right] + \frac{ah}{T}\left\{\begin{array}{l} \frac{b\sim^2 T^{2+3}}{(+1)(2+3)} - \frac{\sim^2 T^{2+2}}{2(+1)^2} \\ -\frac{b\sim T^{+3}}{(+1)(+3)} \\ +\frac{\sim T^{+2}}{(+1)(+2)} - \frac{bT^3}{3} + \frac{T^2}{2} \end{array}\right\} \end{array}\right) \tag{11}$$

Inventory model

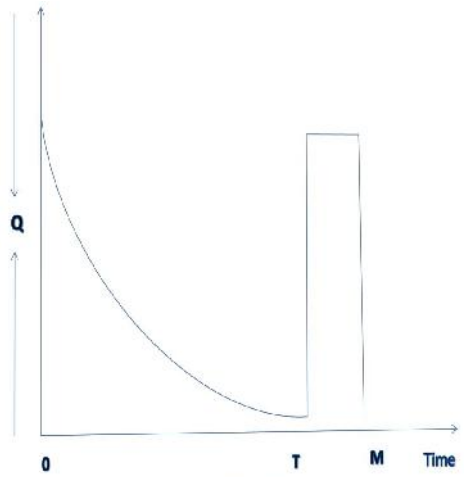

Fig -2 (M ≥ T)

CASE 2: (M ≥ T)

Here, the retailer sells R (T) T-units in all by the of cycle time and has CR (T) T to pay the supplier in full by the end of the credit period M. Hence, interest charges

$$IC_2 = 0 \tag{12}$$

and the interest earned per time unit is

$$IE_2 = \frac{PI_e}{T}\int_0^T R(t)tdt + R(T)T(M-T)$$

$$= \frac{PI_e}{T}\int_0^T a(1-bt)tdt + a(1-bt)T(M-T)$$

$$= \frac{PI_e}{T}\left\{a\left[\frac{t^2}{2}\right]_0^T - ab\left[\frac{t^3}{3}\right]_0^T + aTM - aT^2 - abT^2 MabT^3\right\}$$

$$IE_2 = \frac{aPI_e}{T}\left\{\frac{2bT^3}{3} + TM - \left(\frac{1}{2} + bM\right)T^2\right\} \tag{13}$$

So the total cost $K_2(T)$ of an inventory system for M ≥ T per time unit is

$$K_2(T) = OC + DC + HC + IC_2 - IE_2 - S$$

$$K_2(T)=\left\{\begin{array}{l}\dfrac{A}{T}+\dfrac{a\sim C}{T}\left[\dfrac{T^{+1}}{+1}-\dfrac{bT^{+2}}{+2}\right]-\dfrac{aPI_e}{T}\left\{\dfrac{2bT^3}{3}+TM-\left(\dfrac{1}{2}+bM\right)T^2\right\}\\ +\dfrac{ah}{T}\left\{\begin{array}{l}\dfrac{b\sim{}^2T^{2\ +3}}{(\ +1)(2\ +3)}-\dfrac{\sim{}^2T^{2\ +2}}{2(\ +1)^2}\\ -\dfrac{b\sim\ T^{\ +3}}{(\ +1)(\ +3)}\\ +\dfrac{\sim\ T^{\ +2}}{(\ +1)(\ +2)}-\dfrac{bT^3}{3}+\dfrac{T^2}{2}\end{array}\right\}-\dfrac{¥a\sim C}{T}\left[\dfrac{T^{\ +1}}{+1}-\dfrac{bT^{\ +2}}{+2}\right]\end{array}\right\} \quad (14)$$

Total cost of the inventory system M = T per time can be calculated as

$$K_1(M)=K_2(M)=\left\{\begin{array}{l}\dfrac{A}{M}+\dfrac{a\sim C}{M}\left[\dfrac{M^{\ +1}}{+1}-\dfrac{bM^{\ +2}}{+2}\right]-\dfrac{aPI_e}{M}\left\{\dfrac{2bM^{\ 3}}{3}+M^{\ 2}-\left(\dfrac{1}{2}+bM\right)M^{\ 2}\right\}\\ +\dfrac{ah}{M}\left\{\begin{array}{l}\dfrac{b\sim{}^2M^{\ 2\ +3}}{(\ +1)(2\ +3)}-\dfrac{\sim{}^2M^{\ 2\ +2}}{2(\ +1)^2}\\ -\dfrac{b\sim\ M^{\ +3}}{(\ +1)(\ +3)}\\ +\dfrac{\sim\ M^{\ +2}}{(\ +1)(\ +2)}-\dfrac{bM^{\ 3}}{3}+\dfrac{M^{\ 2}}{2}\end{array}\right\}-\dfrac{¥a\sim C}{M}\left[\dfrac{M^{\ +1}}{+1}-\dfrac{bM^{\ +2}}{+2}\right]\end{array}\right\}$$

$$K_1(M)=K_2(M)=\frac{1}{M}\left\{\begin{array}{l}A+a\sim C\left[\dfrac{M^{\ +1}}{+1}-\dfrac{bM^{\ +2}}{+2}\right]-aPI_e\left\{\dfrac{2bM^{\ 3}}{3}+M^{\ 2}-\dfrac{1}{2}M^{\ 2}-bMM^{\ 2}\right\}\\ +ah\left\{\begin{array}{l}\dfrac{b\sim{}^2M^{\ 2\ +3}}{(\ +1)(2\ +3)}-\dfrac{\sim{}^2M^{\ 2\ +2}}{2(\ +1)^2}\\ -\dfrac{b\sim\ M^{\ +3}}{(\ +1)(\ +3)}\\ +\dfrac{\sim\ M^{\ +2}}{(\ +1)(\ +2)}-\dfrac{bM^{\ 3}}{3}+\dfrac{M^{\ 2}}{2}\end{array}\right\}-¥a\sim C\left[\dfrac{M^{\ +1}}{+1}-\dfrac{bM^{\ +2}}{+2}\right]\end{array}\right\}$$

$$K_1(M)=K_2(M)=\frac{1}{M}\left\{\begin{array}{l}A+a\sim C\left[\dfrac{M^{\ +1}}{+1}-\dfrac{bM^{\ +2}}{+2}\right]-aPI_e\left\{\dfrac{2bM^3}{3}-\left(bM-\dfrac{1}{2}\right)M^2\right\}\\ +ah\left\{\begin{array}{l}\dfrac{b\sim{}^2M^{2\ +3}}{(\ +1)(2\ +3)}-\dfrac{\sim{}^2M^{2\ +2}}{2(\ +1)^2}\\ -\dfrac{b\sim\ M^{\ +3}}{(\ +1)(\ +3)}\\ +\dfrac{\sim\ M^{\ +2}}{(\ +1)(\ +2)}-\dfrac{bM^3}{3}+\dfrac{M^2}{2}\end{array}\right\}-¥a\sim C\left[\dfrac{M^{\ +1}}{+1}-\dfrac{bM^{\ +2}}{+2}\right]\end{array}\right\} \quad (15)$$

For minimizing total cost $K_1(T)$ we need to find and solve partial derivative of it T with Respect to, so

$$\frac{\partial K_1(T)}{\partial T} = \left(\begin{array}{l} -\left(\frac{\sim T^{\ +1}}{\ +1} - \frac{b\sim(\ \ +1)T}{\ +2} - \frac{b}{2} \right)\left(M - \frac{\sim M^{\ +1}}{\ +1} \right) \\ -\frac{A}{T^2} + aCI_c \left\{ -\frac{1}{T^2} \left(\begin{array}{l} -\frac{\sim\ M^{\ +2}}{(\ \ +1)(\ \ +2)} + \frac{M^2}{2} - \frac{bM^3}{6} + \frac{b\sim\ M^{\ +3}}{2(\ \ +2)(\ \ +3)} \\ -\frac{\sim^2 M^{2\ +2}}{(\ \ +1)(2\ \ +2)} + \frac{b\sim^2 M^{2\ +3}}{(\ \ +2)(2\ \ +3)} \end{array} \right) \right\} \\ +a\sim C\left[\frac{T^{\ -1}}{\ +1} - \frac{b(\ \ +1)T}{\ +2} \right] - \frac{aPI_e}{T^2}\left(\frac{M^2}{2} - \frac{bM^3}{3} \right) - ¥a\sim C\left[\frac{T^{\ -1}}{\ +1} - \frac{b(\ \ +1)T}{\ +2} \right] \\ +(ah + aCI_c)\left\{ \begin{array}{l} \frac{b\sim^2(2\ \ +2)T^{2\ +1}}{(\ \ +1)(2\ \ +3)} - \frac{\sim^2(2\ \ +1)T^2}{2(\ \ +1)^2} \\ -\frac{\sim\ b(\ \ +2)T^{\ +1}}{(\ \ +1)(\ \ +3)} \\ +\frac{\sim\ (\ \ +1)T}{(\ \ +1)(\ \ +2)} - \frac{2bT}{3} + \frac{1}{2} \end{array} \right. \end{array} \right)$$

$$K_1(T) = \left(\begin{array}{l} \frac{aCI_c}{T}\left\{ \begin{array}{l} \frac{T^2}{2} - \frac{bT^3}{3} + \frac{\sim T^{\ +2}}{(\ \ +1)(\ \ +2)} - \frac{\sim^2 T^{2\ +2}}{2(\ \ +1)^2} \\ -\frac{b\sim\ T^{\ +3}}{2(\ \ +1)(\ \ +3)} + \frac{b\sim^2 T^{2\ +3}}{(\ \ +1)(2\ \ +3)} \\ -\left(\frac{\sim T^{\ +1}}{\ +1} - \frac{b\sim T^{\ +2}}{\ +2} - \frac{bT^2}{2} + T \right)\left(M - \frac{\sim M^{\ +1}}{\ +1} \right) \\ -\frac{\sim\ M^{\ +2}}{(\ \ +1)(\ \ +2)} + \frac{M^2}{2} - \frac{bM^3}{6} + \frac{b\sim\ M^{\ +3}}{2(\ \ +2)(\ \ +3)} \\ -\frac{\sim^2 M^{2\ +2}}{(\ \ +1)(2\ \ +2)} + \frac{b\sim^2 M^{2\ +3}}{(\ \ +2)(2\ \ +3)} \end{array} \right. + \frac{A}{T} + \frac{a\sim C}{T}\left[\frac{T^{\ +1}}{\ +1} - \frac{bT^{\ +2}}{\ +2} \right] \\ +\frac{aPI_e}{T}\left(\frac{M^2}{2} - \frac{bM^3}{3} \right) - \frac{¥a\sim C}{T}\left[\frac{T^{\ +1}}{\ +1} - \frac{bT^{\ +2}}{\ +2} \right] + \frac{ah}{T}\left\{ \begin{array}{l} \frac{b\sim^2 T^{2\ +3}}{(\ \ +1)(2\ \ +3)} - \frac{\sim^2 T^{2\ +2}}{2(\ \ +1)^2} \\ -\frac{b\sim\ T^{\ +3}}{(\ \ +1)(\ \ +3)} \\ +\frac{\sim\ T^{\ +2}}{(\ \ +1)(\ \ +2)} - \frac{bT^3}{3} + \frac{T^2}{2} \end{array} \right. \end{array} \right) \quad (16)$$

For minimizing total cost $K_2(T)$ we need to find and solve partial derivative of it T with Respect to, so

$$K_2(T)=\left\{\begin{array}{l}\dfrac{A}{T}+\dfrac{a\sim C}{T}\left[\dfrac{T^{+1}}{+1}-\dfrac{bT^{+2}}{+2}\right]-\dfrac{aPI_e}{T}\left\{\dfrac{2bT^3}{3}+TM-\left(\dfrac{1}{2}+bM\right)T^2\right\}\\ +\dfrac{ah}{T}\left\{\begin{array}{l}\dfrac{b\sim{}^2T^{2\ +3}}{(\ +1)(2\ +3)}-\dfrac{\sim{}^2T^{2\ +2}}{2(\ +1)^2}\\ -\dfrac{b\sim\ T^{+3}}{(\ +1)(\ +3)}\\ +\dfrac{\sim\ T^{+2}}{(\ +1)(\ +2)}-\dfrac{bT^3}{3}+\dfrac{T^2}{2}\end{array}\right\}-\dfrac{¥a\sim C}{T}\left[\dfrac{T^{+1}}{+1}-\dfrac{bT^{+2}}{+2}\right]\end{array}\right\}$$

$$K_2(T)=\left\{\begin{array}{l}AT^{-1}+a\sim CT^{-1}\left[\dfrac{T^{+1}}{+1}-\dfrac{bT^{+2}}{+2}\right]-aPI_eT^{-1}\left\{\dfrac{2bT^3}{3}+TM-\left(\dfrac{1}{2}+bM\right)T^2\right\}\\ +ahT^{-1}\left\{\begin{array}{l}\dfrac{b\sim{}^2T^{2\ +3}}{(\ +1)(2\ +3)}-\dfrac{\sim{}^2T^{2\ +2}}{2(\ +1)^2}\\ -\dfrac{b\sim\ T^{+3}}{(\ +1)(\ +3)}\\ +\dfrac{\sim\ T^{+2}}{(\ +1)(\ +2)}-\dfrac{bT^3}{3}+\dfrac{T^2}{2}\end{array}\right\}-¥a\sim CT^{-1}\left[\dfrac{T^{+1}}{+1}-\dfrac{bT^{+2}}{+2}\right]\end{array}\right\}$$

$$K_2(T)=\left\{\begin{array}{l}AT^{-1}+a\sim C\left[\dfrac{T}{+1}-\dfrac{bT^{+1}}{+2}\right]-aPI_e\left\{\dfrac{2bT^2}{3}+M-\left(\dfrac{1}{2}+bM\right)T\right\}\\ +ah\left\{\begin{array}{l}\dfrac{b\sim{}^2T^{2\ +2}}{(\ +1)(2\ +3)}-\dfrac{\sim{}^2T^{2\ +1}}{2(\ +1)^2}\\ -\dfrac{b\sim\ T^{+2}}{(\ +1)(\ +3)}\\ +\dfrac{\sim\ T^{+1}}{(\ +1)(\ +2)}-\dfrac{bT^2}{3}+\dfrac{T}{2}\end{array}\right\}-¥a\sim C\left[\dfrac{T}{+1}-\dfrac{bT^{+1}}{+2}\right]\end{array}\right\}$$

$$\frac{\partial K_2(T)}{\partial T} = \left\{ \begin{array}{l} -\frac{A}{T^2} + a\sim C\left[\frac{T^{-1}}{+1} - \frac{b(\ +1)T}{+2} \right] - aPI_e \left\{ \frac{4bT}{3} - \left(\frac{1}{2} + bM \right) \right\} \\ + ah \left\{ \begin{array}{l} \frac{b\sim^2(2\ +2)T^{2\ +1}}{(\ +1)(2\ +3)} - \frac{\sim^2(2\ +1)T^2}{2(\ +1)^2} \\ -\frac{b\sim\ (\ +2)T^{\ +1}}{(\ +1)(\ +3)} \\ +\frac{\sim\ (\ +1)T}{(\ +1)(\ +2)} - \frac{2bT}{3} + \frac{1}{2} \end{array} \right\} - ¥a\sim C\left[\frac{T^{-1}}{+1} - \frac{b(\ +1)T}{+2} \right] \end{array} \right\}$$

$$\frac{\partial K_2(T)}{\partial T} = \left\{ \begin{array}{l} -\frac{A}{T^2} + a\sim C\left[\frac{T^{-1}}{+1} - \frac{b(\ +1)T}{+2} \right] - aPI_e \left\{ \frac{4bT}{3} - \frac{1}{2} - bM \right\} \\ + ah \left\{ \begin{array}{l} \frac{b\sim^2(2\ +2)T^{2\ +1}}{(\ +1)(2\ +3)} - \frac{\sim^2(2\ +1)T^2}{2(\ +1)^2} \\ -\frac{b\sim\ (\ +2)T^{\ +1}}{(\ +1)(\ +3)} \\ +\frac{\sim\ (\ +1)T}{(\ +1)(\ +2)} - \frac{2bT}{3} + \frac{1}{2} \end{array} \right\} - ¥a\sim C\left[\frac{T^{-1}}{+1} - \frac{b(\ +1)T}{+2} \right] \end{array} \right\} \quad (17)$$

5. NUMERICAL EXAMPLE

Example 1:

Let a=1000, b = 0.2, A = 250, C = 20, P = 40, h = 1, I_c = 0.12, I_e = 0.09, M = 30/365, α = 0.1, β = 2 with proper units we get T_1=0.329 years which is greater then M= 0.082 years. Hence corresponding minimum cost is $K_1(T_1)$ = $ 1345.53 and optimum procurement units are 335.

Example 2:

Let a=600, b = 0.1, A = 50, C = 30, P = 35, h = 1, I_c = 0.15, M = 60/365, α = 0.15, β = 2 with proper units we get T_2=0.16432years which is less then M= 0.082 years. Hence corresponding minimum cost is $K_2(T_2)$ = $ 118.349 and optimum purchase units are 91 units.

6. CONCLUSION

The inventory model for deteriorating items in a declining market with salvage value the effect of delay period offered by the supplier to retailer is analyzed when the demand of the product is decreasing in the market. The amount of inventory is deteriorated at the Weibull deterioration rate. It is observed that the deterioration parameter β, rate of interest charged and purchase cost are more sensitive for the case when credit period is less then the cycle period. And for the other case deterioration parameter β interest rate earned, selling cost and holding cost are more sensitive.

==========

BIBLIOGRAPHY

[1] Aderohunmu, R., Mobolurin, A., Bryson, N. (1995) Joint vendor–buyer policy in JIT manufacturing, J. Oper. Res. Soc. 46, 375–385

[2] Banerjee, A., (1986). A joint economic-lot-size model for purchaser and vendor. Decision sciences, 1986, 292-311.

[3] Billington, P.J. (1987) the classical economic production quantity model with setup cost as a function of capital expenditure, Dec. Sci. 18, 25–42.

[4] Bose, S., Goswami, A. and Chaudhuri, K. S., (1995). An EOQ model for deteriorating items with linear time dependent demand rate and shortages under inflation and time discounting. Journal of the OperationalResearch Society, 46 (6), 771 – 782.

[5] Bringham, E. F. (1995): Fundamentals of financial Management. The Dryden Press, Florida .

[6] Chang, H. J., Teng, J. T., Ouyang, L. Y. and Dye, C. Y. (2006): Retailer's optimal pricing and lot-sizing policies for deteriorating items with partial backlogging. European Journal of Operational Research, 168, 51 – 64.

[7] Chakravarty, A.K., Martin, G.E., (1988). An optimal joint buyer-seller discount pricing model. Computers and Operations Research, 15, 271-281.

[8] Chung, K.J. and Huang, Y.F., (2003). The optimal cycle time for EPQ inventory model under permissible delay in payments. International Journal of Production Economics, 84(3), 30-318.

[9] Dave, U. and Patel, L. K., (1981). (T, Si) – Policy inventory model for deteriorating items with time proportional demand. Journal of the Operational Research Society, 32, 137 – 142.

[10] Dave, U. (1985): On "Economic order quantity under conditions of permissible delay in payments" by Goyal, Journal of the Operational Research Society, 36, 1069.

[11] Donaldson, W. A., (1977). Inventory replenishment policy for a linear trend in demand – an analytical solution. Operational Research Quarterly, 28, 663 – 670.

[12] Goyal, S. K. (1985): Economic order quantity under conditions of permissible delay in payments. Journal of the Operational Research Society, 36, 335 – 338.

[13] Goyal, S. K., (1988). A heuristic for replenishment of trended inventories considering shortages. Journal of the Operational Research Society, 39, 885 – 887.

[14] Goyal, S.K., Gupta, Y.P., (1989). Integrated inventory and models: the buyer vendor coordination, European Journal of Operational Research, 41, 261-269.

[15] Goyal, S. K. and Giri, B. C., (2001). Recent trends in modeling of deteriorating inventory. European Journal of Operational Research, 134, 1 – 16.

[16] Hollier, R. H. and Mak, K.L., 1983. Inventory replenishment policies for deteriorating items in declining market. International Journal of Production research, 21, 813-826.

[17] Huang, C.K. (2002) An integrated vendor–buyer cooperative inventory model for items with imperfect quality, Prod. Plan. Control 13, 355–361.

[18] Huang, Y.F. (2003) optimal retailer's ordering policies in the EOQ model under trade credit financing, J. Oper. Res. Soc. 54, 1011– 1015.

[19] Huang, Y.F. (2006) an inventory model under two levels of trade credit and limited storage space derived without derivatives, Appl. Math. Model. 30, 418–436.

[20] Manoj Kumar Meher, Gobinda Chandra Panda, Sudhir Kumar Sahu, (2012). An inventory model with weibull deterioration rate under the delay in payment in demand declining Market, 6 (23), 1121-1133.

Ms. K. Muthulakshmi, M.Sc., B.Ed., M.Phil.
Lecturer in Mathematics
Department of Mathematics
Theni Kammavar Sangam College of Technology
Theni 625 534
Tamil Nadu
India
mkmuthulaxmi2008@gmail.com

==========
Engineering & Technology in India www.engineeringandtechnologyinindia.com
Vol. 1:2 March 2016
==========

EXPERIMENTAL INVESTIGATION OF EMISSION CONTROL IN IC ENGINES BY INTRODUCING VARIOUS TECHNIQUES

Rajeshkumar G., Rajapandian R., Surendrakumar G., Ananthakumar P., Vasanthaseelan S., and Senthil Ganesh A.

==========

ABSTRACT

Now-a-days the automobiles are very essential needs of human beings. The world without automobiles is unimaginable at present. But the major problem corresponding to the automobiles are unwanted emissions from the engine exhaust. The unwanted emission contains CO, CO_2, HC, SO_X, NO_X, etc. Control of these gases is very essential now, because it leads to harmful injuries to living beings and environment. So, we are going to introduce four methods to reduce these exhaust emissions. These are adding additives methods. In this, we add the 2- ethoxy ethanol and 2- methoxy ethanol with fossil fuels which can reduce the of CO_2 gas emission from the vehicles. Then HHO technology may be used to improve the fuel consumption & reduce CO_2, NO_X level during the combustion process. Then the exhaust gas is treated with the main technology, called charcoal absorber to reduce the CO, HC levels and NaOH silencer reduces more than two-thirds of carbon dioxide.

Keywords: 2-Ethoxy Ethanol, 2-Methoxy Ethanol, Baking Soda, Perforated Tube, Activated Charcoal and HHO.

1. INTRODUCTION

The advent of “first generation” catalytic converters in 1975 significantly reduced hydrocarbon and carbon monoxide emissions. The use of converters provided a huge indirect benefit as well. Because lead inactivates the catalyst, 1975 saw the widespread introduction of unleaded fuels. This resulted in dramatic reductions in ambient lead levels and alleviated many serious environmental and human health concerns associated with lead pollution The next major milestone in vehicle emission control technology came in 1980- 81. In response to tighter standards,

manufacturers equipped new cars with even more sophisticated emission control systems. These systems generally include a "three-way" catalyst (which converts carbon monoxide and hydrocarbons to carbon dioxide and water, and also helps reduce nitrogen oxides to elemental nitrogen and oxygen), plus an on-board computer and oxygen sensor.

Here, in this paper we are using various technologies to reduce unwanted emissions. The technologies like adding additives are initially by the addition of 2- ethoxy ethanol and 2- methoxy ethanol with fossil fuels which can reduce the of CO_2 gas emission from the vehicles. Then HHO technology to improve the fuel consumption & reduce CO_2, NO_X level during the combustion process. Then the exhaust gas was treated with the main technology charcoal absorber to reduce the CO, HC level and NaOH silencer reduces more than two in third of carbon dioxide. We are using these technologies like additives, activated charcoal does not affect the human beings. We are must be avoided all the toxic gases by using various technologies. Composition of the normal petrol engine exhaust is as follows:

- Nitrogen (71% of vol.)
- Carbon dioxide (14% of vol.)
- Water vapour (12% of vol.)
- Oxides of nitrogen (<0.25% of vol.)
- Carbon monoxide (1-2% of vol.)
- Hydrocarbons (<0.25% of vol.)
- Oxides of sulphur (<0.03% of vol.)

2. EXPERIMENTAL SETUP

1. HHO Gas Instead of Inlet Air

Hydrogen is a combustible gas and water on electrolysis splits into two molecules of hydrogen and one molecule of oxygen, hydrogen and oxygen though evolve separately in the electrolysis setup but combines immediately to form Oxy-hydrogen gas(HHO) or commonly called as Brown's gas in the collection tube. On introduction of the brown's gas and air fuel mixture through the air-inlet manifold of the carburettor into the IC engine, the highly flammable Browns gas ignites a fraction of a second earlier than the fuel. No flash points, explosive points or temperatures soaring, takes place during the combustion within the cylinder. The flame speed of hydrogen is very

high compared to that of gasoline. Hence there is no delay in combustion between two points in the cylinder ensuring a smoother performance, this helps in uniform and complete combustion of the additive and fuel mixture inside the cylinder of the engine. In addition to this the life and performance of the engine improves. And because of the complete combustion of the fuel and Browns gas mixture, it ensures that there are no unburned hydrocarbons and also oxidizes the partially oxidized carbon i.e. carbon monoxide (CO) into completely oxidized carbon dioxide (CO_2) which is less harmful compared to carbon monoxide. This results in significant decrease in hydro carbon level in the exhaust of the engine. The brown's gas doesn't cause any pollution as the product after combustion is steam. The brown's gas is liberated using the electrolysis process, where the current is passed through the solution of distilled water and potassium hydroxide(electrolyte), this liberated volume of brown's gas directly depends on

i. Concentration of Electrolyte.

ii. Current sent into the solution.

iii. Area of contact between the electrode and the solution

a) Production of HHO gas

HHO gas is produced by electrolysis of water. The process involves mixing of NAOH/KOH with water in 20% to 30% in order to increase the boost up the electrolysis these two catalysts were mainly chosen because of their easy availability and doesn't affect chemically. Initially container must be chosen, according to engine we selected here we chosen container of volume minimum 10L and now the volume of water taken for electrolysis depends on the engine volume, for example if we choose the sumo engine of 3.0L(engine capacity will be 3000CC) water taken must be above 6000CC (1CC = 1ml) but not to exceed 7000CC. Here we taken 800 CC engine and volume of water taken for electrolysis is 2000CC (2L) and about NAOH taken for dilution in water is about 25% of volume of water i.e.250gms. Now the electrolyte solution (Mixture of NAOH and water) needed for electrolysis is made ready.

Figure 1. Brown Gas Setup Figure 2. Brown Gas Production

2. Adding Additives to the Fuel

There were wide range of additives available to mix with the fuel but here we selected 2-ethoxy ethanol and 2-methoxy ethanol. It's because additives chosen must be oxygenated group of chemicals. Oxygenated fuel is nothing more than fuel that has a chemical compound containing oxygen. It is used to help fuel burn more efficiently and cut down on some types of atmospheric pollution. In many cases, it is credited with reducing the smog problem in major urban canters. It can also reduce deadly carbon monoxide emissions. Oxygenated fuel works by allowing the gasoline in vehicles to burn more completely. Because more of the fuel is burning, there are fewer harmful chemicals released into the atmosphere. In addition to being cleaner burning, oxygenated fuel also helps cut down on the amount of non-renewable fossil fuels consumed.

Figure 3. Additives

a) Properties of Additives Selected

Here we selected 2 – ethoxy ethanol and 2 – methoxy methanol as additive to be mixed or blended with fossil fuel in 9:1 proportion where 9 represents ratio of fuel and 1 represent ratio of additive mixed. In the ratio of additive since we are mixing two different additives, the ratio of mixture varies as .5:.5, .25:.75, .75:.25 by mixing the additives at various proportion we can found the series of variable results.

i. Properties of 2 – ethoxy ethanol

2-Ethoxyethanol is a common solvent. It, like other glycol ethers, is used in the semiconductor industry. It is also used in surface coatings such as lacquers and paints. It is used in varnish removers, printing inks, duplicating fluids, wood stains, and epoxies.

ii. Properties of 2 – methoxy ethanol

2-Methoxyethanol is used as a jet fuel de-icer. It is also used as a solvent for cellulose acetate, resins, dyes, and quick drying varnishes, enamels, nail polishes and wood stains. 2-Methoxyethanol dissolves readily in water and most organic solvents. It is flammable. It is a colourless, flammable, liquid, organic solvent.

3. Charcoal Absorber

Basically a charcoal absorber consists of a perforated tube which is installed at the end of the exhaust pipe. The perforated tube may have holes of different diameters. The very purpose of providing different diameter hole is to break up gas mass to form smaller gas bubbles. Generally 4 sets of holes are drilled on the perforated tube. Around the circumference of the perforated tube a layer of activated charcoal is provided and further a PVC pipe covers it. Also a filler plug is mounted at the both end of the container. At the inlet of the exhaust pipe a non-return valve is provided which prevents the back flow of gases.

Figure 4. Perforated Tube

a) Absorption Process

As the exhaust gases enter in to the charcoal absorber, the perforated tube converts high mass bubbles in lo low mass bubbles after that they pass through charcoal layer which again purify the gases. It is highly porous and posses extra free valences so it has high absorption capacity. Activated charcoal is available in granular or powdered form. As it is highly porous and Possess free valences. So, it possesses high absorption capacity.

Activated carbon is more widely used for the removal of taste and odorous from the public water supplies because it has excellent properties of attracting gases, finely divided solid particles and phenol type impurities, The activated carbon, usually in the powdered form is added to the water

either before or after the coagulation with sedimentation. But it is always added before filtration. Feeding devices are similar to those used in feeding the coagulants.

4. NaOH Silencer

This is the main technology for reduction of CO_2 emission in automobiles. It is a simple design and inexpensive. The emission particles will be absorbed in this technology; nearly about two in third of CO_2 gases will be absorbed in NaOH silencer.

a) Principle

The basic principle of NaOH silencer is the conversion of sodium hydroxide into sodium bicarbonate. The purified exhaust gas from charcoal absorber enters into the special arrangement called NaOH silencer. It's like a hollow cylinder through which layers of binder are rolled inside the cylinder. The cylinder surfaces have small holes throughout the binders. The binders are made by sodium hydroxide (NaOH). These NaOH directly react with CO_2 and forms $NaCO_3$.

$$\mathbf{2NaOH + CO_2 \rightarrow Na_2CO_3 + H_20}$$

These colloidal forms of sodium carbonate ($NaCO_3$) react with CO_2 and forms sodium bicarbonate or sodium hydrogen carbonate ($NaHCO_3$).The sodium bicarbonate is fully in solid form. It is also called as baking soda and it is utilized for day to day life. In this method, the toxic gases like CO_2 are converted into useful works.

$$\mathbf{Na_2CO_3 + H_2O + CO_2 \rightarrow 2NaHCO_3(s)}$$

b) Construction and Working

The NaOH silencer consists of cylindrical container & the NaOH powder is mixed with water. This NaOH silencer is fitted with exhaust pipe line in order to absorb CO_2 from exhaust gasses. In this, cylindrical container carrying NaOH mixture to absorb the CO_2 in the exhaust from the charcoal absorber and also cylindrical container have exhaust port, because after absorbing CO_2 the exhaust gas leaving the system to the atmosphere.

In previous technology we can reduce some amount of emission. But enormous amount of emission causing harmful effect gas like CO_2 can be reduced using NaOH silencer. The low velocity of exhaust gas enters into the NaOH silencer. The velocity of exhaust gas increases with the help of small holes in the arrangement of inlet pipe. The high velocity exhaust gases react with NaOH

mixture. This exhaust gas contains CO_2 gas which may react with NaOH mixture and forms $NaCO_3$ in colloidal form further the CO_2 gas reacted with mixture repeatedly and forms $NaHCO_3$.

The exhaust gases before entering NaOH silencer involves some technology like adding additives and HHO technology. When it is treated, exhaust gases comes out with low temperature compared to the normal technology. This is an important advantage of our NaOH silencer, because if a high temperature gas enters into the purifier it affects the sodium carbonate reaction. But this problem will not occur in the NaOH silencer. Another advantage of this NaOH silencer is, the NaOH are reacted repeatedly with CO_2.

3. EXPERIMENTAL RESULTS

The following table & graph shows the experimental result analysed using flue gas analyser & smoke meter. The results and graphical representations are as follows:

Table 1. Result of Smoke Meter Test and Flue Gas Analyser

EMISSION TEST RESULTS			
Test/ Implementation		**Before Implementation**	**After Implementation**
Smoke Meter Test	Density	10.1 N %	3.8 N %
		0.84 m^{-1}/ ^oC	0.34 m^{-1}/^oC
Flue Gas Analyser	HC	33 PPM	15PPM
	CO	0.07%	0.05%
	CO_2	14%	12%
	NO_X	57 PPM	50 PPM

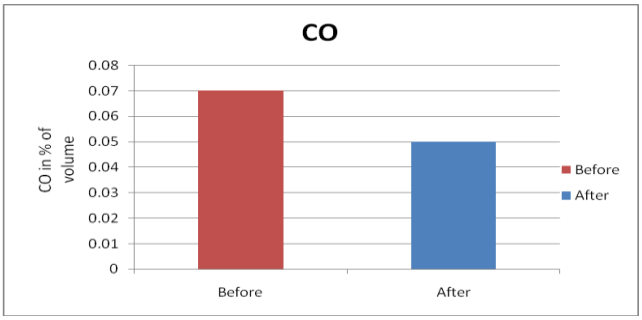

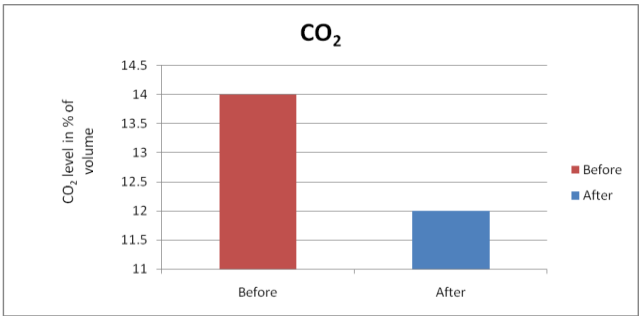

Figure 5. Graphical Representation of CO Emission

Figure 6. Graphical Representation of CO_2 Emission

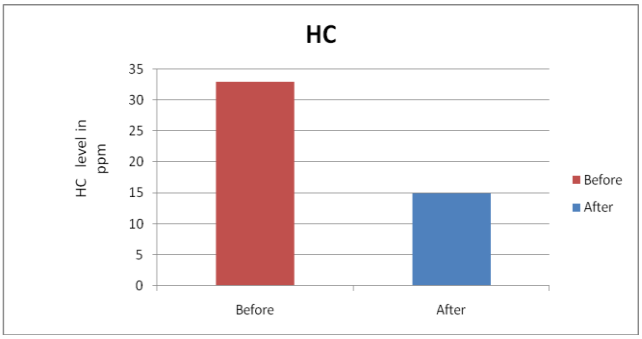

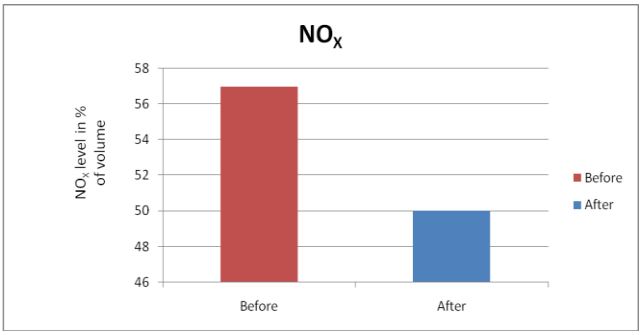

Figure 7. Graphical Representation of HC Emission

Figure 8. Graphical Representation of NO_X Emission

4. CONCLUSION & DISCUSSION

Burning of liquid fuels like petrol, diesel, gasoline etc. result in the emission of toxic gases like CO_2, CO, NO_X, HC etc., From the result of this work we reduced the unwanted emissions from the petrol engine considerably. In this work we are mainly focused on the reduction of CO_2 gas from the exhaust emission. Because CO_2 gas leads to some harmful effects on human beings as well as the environment. The main focuses of the project achieved are as follows,

- Emission control in I.C. Engine and making this setup for commercial use is achieved.
- Compact design and alternative process for current phenomenon is achieved.
- Engine life, Engine efficiency and minimise the fuel consumption also achieved at high rate.

==========

References

1. Ahmad Zaki bin zaimani "*Development hydrogen gas generator for dual fuel engine using yull brown method" 2010*
2. Swastik R. Gajjar, Keval I. Patel "*Design And Development Of Aqua Silencer For Two Stroke Petrol Engine* " International Journal for Innovative Research in Science & Technology (IJIRST) / Vol. 1, Issue 1, June 2014
3. Maryam Mahmoudkhani, David W. Keith "*Low Energy Sodium Hydroxide Recovery for CO_2 Capture from Atmospheric Air- Thermodynamic Analysis* " International Journal of Greenhouse Gas Control-2009
4. M. Al-Hassana, H. Mujafeta and M. Al-Shannag *"An Experimental Study on the Solubility of a Diesel-Ethanol Blend and on the Performance of a Diesel Engine Fueled with Diesel-Biodiesel - Ethanol Blends"* Jordan Journal of Mechanical and Industrial Engineering Volume 6, Number 2, April 2012
5. K.Balasubramaniyan, P.Balashanmugam, A.Raghupathy , G.Balasubramanian *"Studies on Emission Characteristics of Diesel Engine Run Using Diesel Di Methoxy Ethane Blend Fuel"* International Journal of Science, Engineering and Technology Research (IJSETR) Volume 2, Issue 11, November 2013
6. Saed A. Musmar, Ammar A. Al-Rousan "*Effect of HHO gas on combustion emission in gasoline engines*" International Journal of Greenhouse Gas Control, 2011

7. V.Gnanamoorthia, G. Devaradjane *"Effect of Diesel-Ethanol Blends on Performance, Combustion and Exhaust Emission of a Diesel Engine"* International Journal of Current Engineering and Technology, Vol.3, No.1 (March 2013)

8. Natalia Chraplewska, Kamil Duda, Miosz Meus *"Evaluation of usage brown gas generator for aided admission of diesel engine with fermentative biogas and producer gas"* Journal of KONES Power train and Transport, Vol. 18, No. 3 2011.

Rajeshkumar G
Assistant Professor, Mechanical Engineering
Theni Kammavar Sangam College of Technology
Theni 625 534
Tamil Nadu
India
rajesh.mech022@gmail.com

Rajapandian
Assistant Professor, Mechanical Engineering,
Theni Kammavar Sangam College of Technology, Theni.
Theni Kammavar Sangam College of Technology
Theni 625 534
Tamil Nadu
India

R, Surendrakumar G.,
Assistant Professor, Mechanical Engineering,
Theni Kammavar Sangam College of Technology
Theni 625 534
Tamil Nadu
India

Ananthakumar P,
Assistant Professor, Mechanical Engineering,
Theni Kammavar Sangam College of Technology
Theni 625 534
Tamil Nadu
India

Vasanthaseelan S
PG Scholar, Hindustan Institute of Technology
Hindustan University
Chennai
Taminadu
India
vasanthaseelan.s@gmail.com

Senthil Ganesh A
Former UG Scholar
Mechanical Engineering
Theni Kammavar Sangam College of Technology
Theni 625 534
Tamil Nadu
India
mechsenthil19@gmail.com

==========
Engineering & Technology in India www.engineeringandtechnologyinindia.com
Vol. 1:2 March 2016
==========

Person Recognition Using Ear Images

R. Revathi and M. Bhavani

==========

Abstract

We present a complete three-dimensional (3-D) ear recognition system combining local and holistic features in a computationally efficient manner. The system is comprised of four primary components, namely: 1) ear image segmentation; 2) local feature extraction and matching; 3) holistic feature extraction and matching; and 4) a fusion framework combining local and holistic features at the match score level. For the segmentation component, we introduce a novel shape-based feature set, termed the Histograms of Indexed Shapes (HIS), to localize a rectangular region containing the ear. For the local feature extraction and representation component, we extend the HIS feature descriptor to an object-centered 3-D shape descriptor, the Surface Patch Histogram of Indexed Shapes (SPHIS), for local ear surface representation and matching. For the holistic matching component, we introduce a voxelization scheme for holistic ear representation from which an efficient, voxel-wise comparison of gallery-probe model pairs can be made. The match scores obtained from both the local and holistic matching components are fused to generate the final match scores.

Keywords: Histograms of Indexed Shapes, Surface Patch Histogram of Indexed Shapes

INTRODUCTION

BIOMETRICS deals with recognition of individuals based on their physiological or behavioral characteristics. Researchers have done extensive studies on biometrics such as fingerprint, face, palm print, iris, and gait. Ear, a viable new class of biometrics, has certain advantages over face and fingerprint, which are the two most common biometrics in both academic research and industrial applications. For example, the ear is rich in features; it is a stable structure that does not change much with age and it does not change its shape with facial expressions. Furthermore, ear is larger in size compared to fingerprints but smaller as compared to face and it can be easily captured from a distance without a fully cooperative

subject although it can sometimes be hidden with hair, cap, turban, muffler, scarf, and earrings. The anatomical structure of the human ear is shown in Fig. 1.

The ear is made up of standard features like the face. These include the outer rim (helix) and ridges (antihelix) parallel to the helix, the lobe, the concha (hollow part of ear), and the tragus (the small prominence of cartilage over the meatus). In this paper, we use the helix/antihelix for ear recognition.

In this paper, we present a fully automatic, 3-D ear recognition system that combines both local and holistic features in a computationally efficient manner.

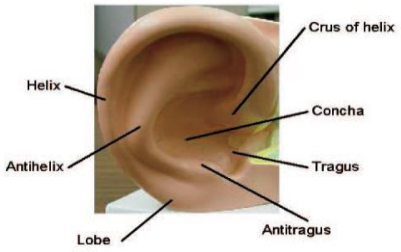

Fig. 1. The external ear and its anatomical parts

The motivation behind combining local and holistic surface features for 3-D ear recognition is that local representations have been found to be more robust to clutter and small amounts of noise, while the holistic representation captures information from the entire surface without excluding any information when describing the ear. When combined effectively, they can provide complementary information describing the 3-D ear shape and jointly enhance the matching performance.

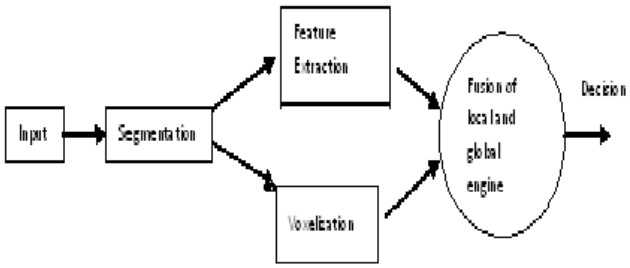

Fig. 2. System overview.

THREE-DIMENSIONAL EAR DETECTION

An overview of our ear detection procedure using the sliding window approach is shown in Fig. 3. To locate the ear in a range image, the image is scanned from the top left corner to the bottom right corner with a fixed-sized detection window. In each window position the HIS feature vector is extracted and employed to train a binary ear/non-ear classifier. The classifier is then used to determine whether the current window contains an ear (positive sample) or non-ear (negative sample) by evaluating the classification score based on the feature vector extracted from the window. SVM is one of the leading techniques used for binary classification due to its robust performance and efficiency in both the training and testing stages.

The scanning window approach employing a fixed-sized window, however, only allows for ear detection at a single scale. To achieve multi-scale detection, the image is gradually resized using a scale factor, and the detection window is then iteratively applied on each of the resized images. After scanning the detection window across the image at multiple scales, multiple detections usually occur around the target regions and it is useful to fuse overlapping detected windows into a single detection [11]. We select a nonmaximal suppression (NMS) method proposed by Dalal [12] as the solution to the fusion of overlapping detected windows, in which each detection is mapped to a respective point in 3-D space (position and scale of the scanning window) weighted by their confidence scores. A nonparametric density estimator is employed to estimate the corresponding density function, where the resulting peaks of the density function constitute the final detections, with positions, scales and confidence scores given by the positions of the peaks. After nonmaximal suppression, the detection system returns a bounding box with an associated detection score representing the ear region.

A. HIS Feature Descriptor

Objects can be characterized by their distinct 3-D surface shapes. The human ear, for instance, contains areas around the helix ring and antihelix that possess both prominent saddle and ridge shapes, while the inner ear regions have rut and trough shapes.

1) Shape Index: A quantitative measure of the shape of a surface at a vertex, called the shape index S_I , is defined as

$$S_I(\mathbf{p}) = \frac{1}{2} - \frac{1}{\pi} \arctan\left(\frac{k_{\max}(\mathbf{p}) + k_{\min}(\mathbf{p})}{k_{\max}(\mathbf{p}) - k_{\min}(\mathbf{p})}\right) \quad (1)$$

where K_{max},K_{min} are the principal curvatures of the surface at vertex , with $K_{max} > K_{min}$ defined as

$$k_{\max}(\mathbf{p}) = H(\mathbf{p}) + \sqrt{H^2(\mathbf{p}) - K(\mathbf{p})} \quad (2)$$
$$k_{\min}(\mathbf{p}) = H(\mathbf{p}) - \sqrt{H^2(\mathbf{p}) - K(\mathbf{p})}. \quad (3)$$

$$K = \frac{(eg - f^2)}{(EG - F^2)} \quad (4)$$
$$H = \frac{(eG - 2fF + gE)}{(2\{EG - F^2\})} \quad (5)$$

$$E = \|\mathbf{x}_u\|^2, \quad F = \mathbf{x}_u\mathbf{x}_v, \quad G = \|\mathbf{x}_v\|^2 \quad (6)$$
$$e = \frac{\det(\mathbf{x}_{uu}\mathbf{x}_u\mathbf{x}_v)}{\sqrt{EG - F^2}}, \quad f = \frac{\det(\mathbf{x}_{uv}\mathbf{x}_u\mathbf{x}_v)}{\sqrt{EG - F^2}}$$
$$g = \frac{\det(\mathbf{x}_{vv}\mathbf{x}_u\mathbf{x}_v)}{\sqrt{EG - F^2}}. \quad (7)$$

2) Curvedness: The shape index of a rigid object is not only independent of its position and orientation in space, but also independent of its scale. To encode the scale information, we utilize the curvedness, which is also known as the bending energy, to capture the scale differences [13]. Mathematically, the curvedness of a surface at a vertex is defined as

$$C_v(\mathbf{p}) = \sqrt{\frac{k_{\max}^2(\mathbf{p}) + k_{\min}^2(\mathbf{p})}{2}}. \quad (8)$$

3) HIS Descriptor: The HIS descriptor is defined using the shape index and curvedness values calculated from the vertices contained within the surface region to be encoded. To build the histogram descriptor, first the curvedness and shape index values are collected at each vertex over the surface region. Each vertex contributes a weighted vote for a histogram bin based on its shape index value, with a strength that depends on its curvedness. The votes

of all vertices are then accumulated into the evenly spaced shape index bins forming the HIS descriptor encoding the shape information over the surface region. To avoid boundary effects, linear interpolation is used to distribute each curvedness value into adjacent shape index histogram bins. Let x and c be the shape index and curvedness values of a 3-D vertex on the surface region which contribute a weighted vote to the HIS histogram,x_1 and $x_2$be the centers of the two nearest neighboring bins of such that ,$x_1 \leq x \leq x_2$ and be a HIS histogram with bins. The linear interpolation method that distributes the vertex's curvedness into the two nearest neighboring bins is defined as follows:

$$h(x_1) = h(x_1) + c\left(1 - \frac{x - x_1}{b}\right) \qquad (9)$$

$$h(x_2) = h(x_2) + c\left(\frac{x - x_1}{b}\right) \qquad (10)$$

B. Feature Encoding for Detection Window

1) Block-Structured HIS: In our detection system using the sliding window approach, the detection window is tiled with blocks of various sizes from which the HIS feature descriptors are built and combined. Fig. 3 explains our feature encoding procedure for the detection window with tiled blocks. For an image window of size 96x64, we construct a feature descriptor based on the histograms of blocks of size 32x32, 16x16, 16x32, and 32x16 overlayed on the image window with an overlap of half a block size. Feature descriptors derived from larger blocks capture holistic details of the input image while features derived from smaller blocks capture finer shape information.

2) Integral HIS*:* In order to efficiently compute the HIS features used by our detector, we make use of the integral histogram method suggested by Porikli [16] for computing histograms over arbitrary rectangular image regions and devise a way for the fast evaluation of HIS features on the blocks. In order to extend the framework of the integral histogram to our detector, we generate for each vertex an 8-D HIS calculated from its own shape index and curvedness values using the method described in Section III-A3. The histogram will consist of only two bins with nonzero values; these are the two adjacent bins that are closest in distance to the shape index of the vertex. The spatial positions of the vertices are then used to propagate an aggregated function of the integral histogram, starting from a point of origin, e.g., top left corner, and traverse through the remaining points. We iterate the integral HIS at

the current vertex using the histograms of the previously processed neighboring points. At each iteration, the values of the integral HIS bins are incremented by the values of the corresponding HIS bins of the current vertex. After the integral HIS is obtained for each vertex, the HIS histogram of a rectangular block can be computed in a constant computational time of an 8-D histogram vector addition and two 8-D histogram vector subtractions, accessing only the integral histogram values at the corner points of those blocks without reconstructing a separate histogram for every block.

LOCAL FEATURE EXTRACTION

A. 3-D Keypoint Detection

To generate the set of local features, the input image is initially searched to identify potential keypoints that are both robust to the presence of image variations and highly distinctive, allowing for correct matching. The keypoint detection method proposed here is inspired by the 3-D face matching approach presented by Mian, *et al.* in [9], but with major enhancements tailored towards improved robustness and applicability to objects with salient curvature, such as the ear. In [9], the input point cloud of the range image is sampled at uniform intervals. By observing 3-D ear images, we found that the majority of these salient points are located in surface regions containing large curvedness values. This signifies that sampling in regions containing large curvedness values will result in a higher probability of obtaining repeatable keypoints. Once a candidate keypoint has been located, a local surface patch surrounding the candidate keypoint is cropped from the ear image using a sphere centered at the candidate keypoint. The purpose of examining its nearby surface data is to further reject candidate keypoints that are less discriminative or less stable due to their location in noisy data or along the image boundary.

B. Local Surface Matching Engine

In our local feature representation, a 3-D ear surface is described by a sparse set of keypoints, and associated with each keypoint is a descriptive SPHIS feature descriptor that encodes the local surface information in an object-centered coordinate system. The objective of the local feature matching engine is to match these individual keypoints in order to match the entire surface. To allow for efficient matching between gallery and probe models, all

gallery images are first processed. The extracted keypoints and their respective SPHIS feature descriptors are stored in the gallery. Each feature represents the local surface information in a manner that is invariant to surface transformation. A typical 3-D ear image will produce approximately 100 overlapping features at a wide range of positions that form a redundant representation of the original surface. In the local feature matching stage, given a probe image, a set of keypoints and their respective SPHIS descriptors are extracted using the same parameters as those used in the feature extraction of the gallery images. If the cropped surface data contains boundary points, the candidate keypoint is rejected automatically as being close to the image boundary. Otherwise, PCA is applied to the cropped surface data, and the eigenvalues and eigenvectors are computed to evaluate its discriminative potential.

1) Surface Patch Histogram of Indexed Shape (SPHIS) Descriptor:

As mentioned in Section III-A3, the HIS descriptor can be used to encode shape information of any surface region. In addition, we can form an HIS of arbitrary size by uniformly spacing the shape index values over the range [0, 1]. The larger the dimensionality of the HIS, the more descriptive it is. However, too large of a descriptor may be sensitive to noise. Based on the HIS descriptor, the SPHIS descriptor is employed to represent the keypoint and is built from the surface patch surrounding it.

IV. HOLISTIC FEATURE EXTRACTION

A. Preprocessing

For a gallery model, the ear surface output from the detection component is normalized to a standard pose. The centroid of the surface is firstly mapped to the origin of the coordinate system. Then, the principal components corresponding to the two largest eigenvalues of the surface are calculated. The surface is then rotated such that the two principal components are aligned with the axes of the coordinate system. The preceding section described the method by which to establish correspondences between a probe-gallery pair. The probe model is then registered onto the gallery model by applying the transformation obtained by the local matching stage for each point on the probe model. In the event that the number of established correspondences is below three, we rely on the pose normalization scheme for the model registration.

The local and holistic matching components result in independent similarity matrices S_i each of size P x G , where I Є {1,2} denotes the matching engine and represents the number of probe and gallery models, respectively. We fuse the local and holistic match scores using the weighted sum technique. This approach is in the category of transform-based techniques (i.e., based on the classification presented in [18]. In practical multimatcher biometric systems, a common fusion method is to directly combine the match scores provided by different matchers without converting them into posteriori probabilities. However, the combination of the match scores is meaningful only when the scores of the individual matchers are comparable. This requires a change of the location and scale parameters of the match score distributions at the outputs of the individual matchers. Hence, the *sigmoid function* score normalization [19], which is proven to be an efficient and robust technique in [18], is used to transform the match scores obtained from the different matchers into a common domain. It is defined as follows:

$$s_j^n = \begin{cases} \frac{1}{1+exp\left(-2\left(\frac{s_j-\tau}{\alpha_1}\right)\right)} & s_j < \tau, \\ \frac{1}{1+exp\left(-2\left(\frac{s_j-\tau}{\alpha_2}\right)\right)} & \text{otherwise} \end{cases} \qquad (11)$$

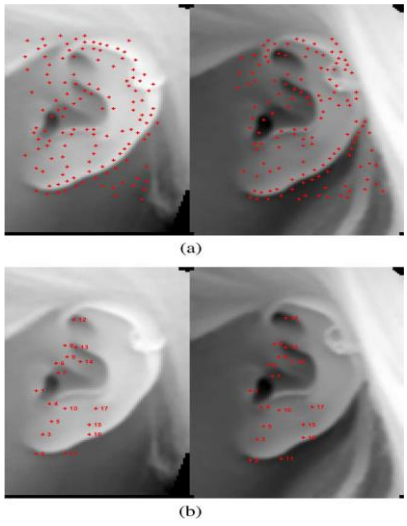

Fig. 3. Example of finding feature correspondences for a pair of gallery and probe ears from same subject. (a) Key points detected on ears. (b) True feature correspondences recovered by local surface matching engine.

V. CONCLUSION

We have presented a complete, automatic 3-D ear biometric system using range images. Within the system, a novel 3-D shape descriptor, the Histogram of Indexed Shapes, is proposed to robustly encode 3-D ear shape and is used in 3-D ear detection and recognition tasks. The proposed 3-D ear surface matching approach employs both local and holistic 3-D ear shape features. The experimental results demonstrate the accuracy and efficiency of our novel 3-D ear shape matching approach. The proposed system achieves a rank-one recognition rate of 98.3% and an EER of 1.7% on a 415-subject dataset with an average time lapse of 17.7 weeks between successive acquisitions of a subject. Moreover, the proposed approach achieves a significantly higher computational efficiency than the SOA systems.

==========

References

[1] H. Chen and B. Bhanu, "Human ear recognition from side face range images," in *Proc. Int. Conf. Pattern Recognition*, Aug. 2004, pp.574–577.

[2] H. Chen and B. Bhanu, "Contour matching for 3-D ear recognition," in *Proc. IEEE Workshop Applications Computer Vision*, Jan. 2005, pp.123–128.

[3] H. Chen and B. Bhanu, "Human ear recognition in 3D," *IEEE Trans.Pattern Anal. Machine Intell.*, vol. 29, no. 4, pp. 718–737, Apr. 2007.

[4] P. Yan and K. Bowyer, "Empirical evaluation of advanced ear biometrics," in *Proc. CVPR 2005—Workshops*, Jan. 2005, pp. 41–41.

[5] P. Yan and K. Bowyer, "Biometric recognition using 3D ear shape," *IEEE Trans. Pattern Anal. Machine Intell.*, vol. 29, no. 8, pp.1297–1308, Aug. 2007.

[6] T. Theoharis, G. Passalis, G. Toderici, and I. Kakadiaris, "Unified 3Dface and ear recognition using wavelets on geometry images," *Pattern Recognition*, vol. 41, no. 3, pp. 796–804, Mar. 2008.

[7] I. Kakadiaris,G.Passalis, G. Toderici, N.Murtuza, Y. Lu, K. N., and T. Theoharis, "3D face recognition in the presence of facial expressions:An annotated deformable model approach," *IEEE Trans. Pattern Anal.Machine Intell.*, vol. 29, no. 4, pp. 640–649, Apr. 2007.

[8] S. Islam, R. Davies, M. Bennamoun, and A. Mian, "Efficient detection and recognition of 3D ears," *Int. J. Computer Vision*, vol. 95, no. 1, pp.52–73, 2011.

[9] A. Mian, M. Bennamoun, and R. Owens, "Keypoint detection and local feature matching for textured 3D face recognition," *Int. J. Computer Vision*, vol. 79, no. 1, pp. 1–12, 2008.

[10] S. Cadavid and M. Abdel-Mottaleb, "3-D ear modeling and recognition from video sequences using shape from shading," *IEEE Trans. Inform.Forensics Security*, vol. 3, no. 4, pp. 709–718, Dec. 2008.

[11] P. Viola and M. Jones, "Robust real-time object detection," *Int. J. Computer Vision*, vol. 57, no. 2, pp. 137–154, 2001.

[12] N. Dalal, "Finding People in Images and Videos," Ph.D. dissertation, Institut National Polytechnique de Grenoble, Grenoble, France, Jul.2006.

[13] C. Dorai and A. Jain, "Cosmos—A representation scheme for 3D freeform objects," *IEEE Trans. Pattern Anal. Machine Intell.*, vol. 19, no.10, pp. 1115–1130, Oct. 1997.

[14] A. Gray, *Modern Differential Geometry of Curves and Surfaces With Mathematica*, 2nd ed. Boca Raton, FL: CRC, 1997.

[15] P. Besl, "Surface in range image understanding," in *Springer Series in Perception Engineering*. New York: Springer-Verlag, 1988.

[16] F. Porikli, "A fast way to extract histograms in Cartesian spaces," in *Computer Vision Pattern Recognition (CVPR)*, 2005.

[17] S. Wang and A. Kaufman, "Volume sampled voxelization of geometric primitives," in *Proc. 4th Conf. Visualization*, 1993, pp. 78–84.

[18] A. Ross, K. Nandakumar, and A. Jain, *Handbook of Multibiometrics (International Series on Biometrics)*. Secaucus, NJ: Springer-Verlag, 2006.

[19] R. Cappelli, D. Maio, and D. Maltoni, "Combining fingerprint classifiers," in *Proc. Fist Int. Workshop Multiple Classifier Systems*, 2000,pp. 351–361.

[20] J. Zhou, S. Cadavid, and M. Abdel-Mottaleb, "Histograms of categorized shapes for 3D ear detection," in *Proc. IEEE Fourth Int. Conf.sep2010.*

==========

R. Revathi
Assistant Professor in Computer Science & Engineering
Theni Kammavar Sangam College of Technology
Theni 625 534

Tamilnadu
India
revavyas@gmail.com

M. Bhavani
Assistant Professor in Computer Science & Engineering
Theni Kammavar Sangam College of Technology
Theni 625 534
Tamilnadu
India
gmbhavani1990@gmail.com\

==========
Engineering & Technology in India www.engineeringandtechnologyinindia.com
Vol. 1:2 March 2016
==========

Face Recognition Using PCA and LDA Algorithm

K. Velkumar and M. Bhavani

==========

Abstract

Security is an important concept in all areas. In computer science, biometrics is used for identification as well as for authentication to provide or control access. Lot of biometric recognitions are available among various biometrics, the face recognition is one of the best approach. For extracting the features of face images the combination of both Linear discriminant analysis and Principal Component Analysis algorithms are used. The ORL database has been used for visible facial images, and CASIA dataset has used for IR facial images. As a result, these combinations of an algorithm provide high recognition rate as well as more security.

Keywords: Linear Discriminant Analysis, Principal Component Analysis

I. INTRODUCTION

Face recognition is used for identifying or verifying the person. Some facial recognition algorithms identify facial features by extracting landmarks, or features, from an image of the subject's face. For example, an algorithm may analyze the relative position, size, and/or shape of the eyes, nose, cheekbones, and jaw.[2] These features are then used to search for other images with matching features.[3] Other algorithms normalize a gallery of face images and then compress the face data, only saving the data in the image that is useful for face recognition. A probe image is then compared with the face data.[4] One of the earliest successful systems[5] is based on template matching techniques[6] applied to a set of salient facial features, providing a sort of compressed face representation. Recognition algorithms can be divided into two main approaches, geometric, which looks at distinguishing features, or photometric, which is a statistical approach that distills an image into values and compares

the values with templates to eliminate variances. Popular recognition algorithms include Principal Component Analysis using eigenfaces, Linear Discriminate Analysis, Elastic Bunch Graph Matching using the Fisherface algorithm, the Hidden Markov model, the Multilinear Subspace Learning using tensor representation, and the neuronal motivated dynamic link matching.

Another emerging trend uses the visual details of the skin, as captured in standard digital or scanned images. This technique, called skin texture analysis, turns the unique lines, patterns, and spots apparent in a person's skin into a mathematical space.[3] Tests have shown that with the addition of skin texture analysis, performance in recognizing faces can increase 20 to 25 percent. [3]

II. VISIBLE AND IR IMAGE FACE RECOGNITION

An Infrared image of a human being's face represents its unique thermal properties which can be used for recognition of his face. The IR images have advantages than visible light images, and used to improve the success rate of techniques used in face recognition of human beings. IR images do not vary in extreme lighting conditions, even if there is complete darkness. These facial images are less affected if there is a change in facial expressions or poses. [12]

Recognition of visible images affects if the illumination conditions varies. Variations in the facial images of one person due to variations in illumination are more than the variations due to change in the identity of a person. Recognition of faces using infrared (IR) images has become an area of growing research. Thermal Infrared images are invariant to changes in illumination, and helps for identification of individuals under different lighting conditions even in complete darkness. [13]

Thermal face recognition helps to identify the faces of persons if there is no control or little control on light conditions. The benefit of using thermal IR imagery on visible imagery is due to the fact, the light in the Infrared range is emitted but not reflected. IR emissions from the skin, independent of illumination, are its intrinsic feature. Thus, thermal IR sensors capture images that does not change when illumination changes. The within-class variations

in IR imagery are also less than in visible light images. The IR range has been found to be more advantageous than the visible range for detection of face, disguised faces, and recognition of face in poor light conditions.

III. RINCIPAL COMPONENT ANALYSIS

Principal Component Analysis (PCA) is a technique of reducing the dimensions, used in compression of data and recognition tasks. It is a Karhunen-Loeve Transformation also known as Eigenspace projection. Kirby and Sirovich[2] used PCA technique for representation of faces and Turk and Pentland[3] extend this technique to recognize the faces. It is a statistical method having applications in fields like image compression and recognizing faces, and is used to find patterns in high dimensional data. In PCA technique, the testing and training images should be of the similar size and normalized also. Then the PCA approach is applied to reveal a low dimensional structure of image by reducing the dimension of the data. By this reduction in dimensions of data only the information which is not useful is removed and it the structure of face into orthogonal (uncorrelated) components, which are not correlated. These components are known as Eigen faces [9].

In this subspace, each face image may be described and represented as a weighted sum of the orthogonal components. The weighted sum is known as a feature vector and each facial image is stored in a 1D array. A testing image is compared with images in database by calculating the distance between their feature vectors. In PCA approach, there is a requirement of the full frontal face image otherwise it gives poor performance. The feature of this technique is that it is able to reduce the data to 1/1000th of data presented needed to identify the individual. The central idea PCA is the dimensionality of data, which consists of large number of interrelated variables and retains maximum variation in the data set, as much as possible. It is the used if a strong correlation exists between the variables. The basis vectors represent the direction in which maximum variation exists in training vectors and are known as eigenvectors, Each vector can be considered as a feature. These vectors are also termed as eigenfaces. The possibility of eigenfaces' number is equal to the images' number in the training set. But it is not feasible to consider all the eigenfaces, so a face can also be represented as the approximation of the best eigenfaces according to the large value of eigenvalues, and these eigenvalues represents the maximum variation in the set of face

images. Then the eigen vectors are sorted in decreasing order of their corresponding eigen values. The eigenvector having largest eigen value represents the maximum variation in the image.

The first Eigen image is the mean image, and the remaining eigen images represents the variations in images from this mean image. The image of a face is projected onto the face space. In the face space, the face is expressed by coefficients of its eigenface. A facial image of having large input vector is computed by using its small weight vector. Original face can be reconstructed having small error, because the the images that need to be compared and other for the images to whom the images will compared namely ,testing set and training set. The training database contains images of 40 persons, having 9 facial images with different expressions of a single person. That is, the training database consists of 360 images. First of all, training of the recognition system is done by selecting the training database, in which there are 40 folders, corresponding to 40 different individuals. Each folder contains 9 facial images with different expressions or poses, of the same person. The database is selected for training, features are extracted and saved and training time is dimensions of the image space are very large as compared to the face space.

IV. LINEAR DISCRIMINANT ANALYSIS

Linear Discriminant Analysis (LDA) is a classification technique used successfully in many pattern recognition problems statistically. It was developed by Ronald Fisher, who was a professor of statistics at University College London, and the technique also called Fisher Discriminant Analysis (FDA). The idea behind LDA is to separate the input samples belonging to different groups. This technique attempts to increase the ratio of the matrix determinant of the between class scatter to the matrix determinant of the within class scatter. Fisher discriminant combines images belonging to the similar class and differentiates images belonging to different classes. Then the images are projected from 2-D space to D dimensional space, where D is equal to different classes of input images.

V. METHODOLOGY

The main challenge in the problem of face recognition system is the variation within the class (intra-class) due to changes in facial expressions, pose, variation in illumination,

which sometimes exceed variation between the classes(inter-class).In other words, different persons looks almost similar in the same pose and one person appears different when viewed in different poses. Similarly, different persons appear almost similar in the same illumination and the same person appears different in different illuminations. Collect a dataset of images, Visible as well as IR images. For each dataset, Form a mean image of dataset, which will be used for making a database. After forming the mean image, next is to apply PCA technique to extract the eigen features and on concept of that, eigenfaces will be formed. On these eigen based images, LDA concept will be applied, which will help to reduce the complexity of feature detection. These features are saved as the database for classification process. Next, same steps will be followed for extracting the features from testing image with different variations. The extracted features are then subtracted from database features A threshold difference is defined to match the faces. Image is recognized as the one which gives the difference less than or equal to the threshold value.

Testing images are compared with the images of training database, to find out how many probe images are matched with the gallery images. Testing or Recognition tine and the recognition rate are calculated.

TABLE 1

S.No.	**System**	**% Recognition Rate**	**Training Time Per Model**	**Testing Time Per Model**
1.	PCA	83	6.52 Sec	2.73sec
2.	LDA	83	7.44 Sec	3.12 Sec
3.	Propose	92.5	39.2 Sec	2.3 Sec

	d Method			

The same procedure is followed on Near Infrared (NIR) Images, and the results are:

TABLE 2

% Recognition Rate	Training Time	Testing Time
97%	39.2 sec	2.3 sec

VII. CONCLUSION

Combining both PCA and LDA techniques will provide strong identity and we will get improved results when compared to other algorithms. The recognition rate for this biometric type will be 97%.

For future work we are trying to combine more than one biometrics for recognition it will provide more security.

==========

References

[1] D. L. Woodard and P. J. Flynn, “Personal identification utilizing finger surface features”, *In Proc. of CVPR-2005*, pp. 1030 – 1036, 2005.

[2] "Airport Facial Recognition Passenger Flow Management". hrsid.com.

[3] Bonsor, K. "How Facial Recognition Systems Work". Retrieved 2008-06-02.

[4] *Smith, Kelly.* "Face Recognition" *(PDF)*. Retrieved 2008-06-04.

[5] R. Brunelli and T. Poggio, "Face Recognition: Features versus Templates", IEEE Trans. on PAMI, 1993, (15)10:1042-1052

[6] R. Brunelli, Template Matching Techniques in Computer Vision: Theory and Practice, Wiley, ISBN 978-0-470-51706-2, 2009 ([1] TM book)

[7] Kresimir Delac, Mislav Grgic, Sonja Grgic, ―Independent Comparative Study of PCA, ICA, and LDA on the FERET Data Set‖, University of Zagreb, FER, Unska 3/XII, Zagreb, Croatia , 1pages 252–260, February 2009.

[8] Shahrin Azuan Nazeer, Nazaruddin Omar, Marzuki Khalid, ―Face Recognition System using Artificial Neural Networks Approach‖, Signal Processing, Communications and Networking, pp.:420-425, Feb 2009.

[9] Zunxiong Liu, Zheng Xu, Linfeng Hu, ―A comparative study of distance metrics used in face recognition‖, Journal of Theoretical and Applied Information Technology Vol 5. No2. on pages: 206-211, 2009.

[10]Issam Dagher, ―Incremental PCA-LDA Algorithm‖, International Journal of Biometrics and Bioinformatics IJBB , Volume: 4, Issue: 2, Publisher: Citeseer, Pages: 86-99, 2010.

[11]Sushma Niket Borade and Dr. Ramesh P. Adgaonkar, ―Comparative Analysis of PCA and LDA‖, 2011 International Conference on Business, Engineering and Industrial Applications, 2011.

[12]Gil Friedrich and Yehezkel Yeshurun, ―Seeing People in the Dark: Face Recognition in Infrared Images‖, 2nd BMCV, Tubingen, 2003.

[13] Seong G. Kong, Jingu Heo, Besma R. Abidi, Joonki Paik, and Mongi A.

Abidi, ―Recent advances in visual and infrared face recognition—a review‖, Imaging, Robotics,

==========

K. Velkumar
Assistant Professor in Computer Science & Engineering
Theni Kammavar Sangam College of Technology
Theni 625 534
Tamil Nadu
India
velkumar1982@yahoo.com

M. Bhavani
Assistant Professor in Computer Science & Engineering
Theni Kammavar Sangam College of Technology
Theni 625 534
Tamil Nadu
India
gmbhavani1990@gmail.com